Elsevier Editorial System(tm) for Journal of Non-Crystalline Solids

Manuscript Draft

Manuscript Number: NOC-D-17-01061R1

Title: Upconversion luminescence of Er3+/Yb3+ and their role in the stabilization of cubic NaLaF4 nanocrystals in transparent oxyfluoride glass ceramics

Article Type: Full Length Article

Keywords: upconversion;
site-selective spectroscopy;
NaLaF4;
oxyfluoride;
glass ceramics

Corresponding Author: Ms. Guna Krieke,

Corresponding Author's Institution: Institute of Solid State Physics

First Author: Guna Krieke

Order of Authors: Guna Krieke; Anatolijs Sarakovskis, Dr.phys; Maris Springis, Dr.phys

Abstract: Novel Er3+ and Yb3+ doped transparent oxyfluoride glass ceramics containing NaLaF4 nanocrystals were prepared from oxyfluoride glasses with general composition of Na2O-NaF-LaF3-Al2O3-SiO2. The crystallization processes, changes in morphology and upconversion luminescence were analyzed. The heat treatment of the precursor glasses promoted the formation of hexagonal NaLaF4 and an unidentified fluorite type compound. An enhancement of upconversion luminescence with the introduction of YbF3 in the glass ceramics was detected and indicated an efficient energy transfer from Yb3+ to Er3+. The local environment of Er3+ in hexagonal NaLaF4 and the fluorite phase was analyzed using site-selective spectroscopy and compared with polycrystalline ceramics. The incorporation of Er3+ ions in three non-equivalent cationic sites in the crystalline lattice of hexagonal NaLaF4 nanocrystals was observed. The local environment of erbium ions in the fluorite phase was found to be similar to α-NaYF4 suggesting the formation of Er3+ and Yb3+ stabilized α-NaLaF4.

Journal of
Non-Crystalline Solids

Confirmation of Authorship

As corresponding author, I Guna Krieke, hereby confirm on behalf of all authors that:

1. This manuscript has not been published, was not, and is not being submitted to any other journal. It has not been presented at a conference or published in conference proceedings.

2. All necessary permissions for publication were secured prior to submission of the manuscript.

3. All authors listed have made a significant contribution to the research reported and have read and approved the submitted manuscript, and furthermore, all those who made substantive contributions to this work have been included in the author list.

***Revision Notes**

Comma included in text (page 2, line 5).

“the” included in text (page 2, line 12 and 13).

Semicolon replaced by comma (page 2, line 18).

“heating” replaced by “the annealing” (page 2, line 19).

Precision of DTA measurements added (page 2, line 25).

Method for calculation unit cell parameters is added in text (page 2 and 3).

Comma included in text (page 3, line 3 and 13).

“in different experiments” included in text (page 3, line 4).

“either a” included in text (page 3, line 4).

“wavelength-tunable” included in text (page 3, line 5).

“or a” included in text (page 3, line 6).

Method for curve fitting is included in text (page 3, line 8-10).

Method for calculation of effective luminescence decay time is added (page 3, line 12-13).

x-axes of DTA curves are extended in Fig. 1

The variation of characteristic temperatures is included in Table 1.

“°C” is included in Table 1.

“of” included in text (page 5, line 6).

Ref. [30] J. Zhao, R. Ma, X. Chen, B. Kang, X. Qiao, J. Du, X. Fan, U. Ross, C. Roiland, A. Lotnyk, L. Kienle, X. Zhang, From Phase Separation to Nanocrystallization in Fluorosilicate Glasses: Structural Design of Highly Luminescent Glass-Ceramics, J. Phys. Chem. C. 120 (2016) 17726–17732. doi:10.1021/acs.jpcc.6b05796. added in the text (page 5 line 10 and 12).

“the” included in text (page 5, line 10).

“In phase separated glasses two or more glass transition temperatures are expected. Unfortunately, in the investigated glasses, no second Tg, corresponding to the glass transition temperature of the fluoride-rich phase could be detected, nevertheless phase separation was detected in TEM analysis discussed further in the text” included in text (page 5, line 16-19).

Comma included in text (page 5, line 22 and 23).

JCPDS patterns of tetragonal and rhombohedral LaOF included in Fig.2.

“It is a cubic fluorite type compound isostructural with cubic LaOF having a unit cell parameter a=5.782±0.006 Å.” Replaced with “It is a fluorite type compound seemingly isostructural with cubic LaOF having a unit cell parameter a=5.782±0.006 Å. Three polymorphic modifications are known for LaOF: high temperature fluorite

type α-LaOF ($Fm\bar{3}m$) and two distorted fluorite phases – rhombohedral β-LaOF ($R\bar{3}m$) and tetragonal γ-LaOF (P4/nmm) [24]. Due to similarities in the crystalline structure of fluorite and distorted fluorite phases, all three modifications agree reasonably well with the XRD pattern. An isostructural crystalline compound has been observed in other glass ceramics [33,34] and the authors identify it as a rhombohedral LaOF based on XRD data despite the absence of the superstructure peaks characteristic to the rhombohedral distortion in fluorite lattice. However, it is often difficult to observe superstructure peaks of related structures especially in nanocrystalline glass ceramics, therefore the identification of such phases should not be based only on XRD data." (page 6-7).

"and" replaced with "using luminescence measurements (site-selective spectroscopy) and will be" in text (page 7, line 5-6).

Table 2 changed form

The crystalline phases in glass ceramics with 0% and 3% YbF_3

Heat treatment	0% YbF_3	3% YbF_3
glass	amorphous	amorphous
500°C	amorphous	$NaLaF_4$+fluorite
600°C	$NaLaF_4$	$NaLaF_4$+fluorite
700°C	$NaLaF_4$+$NaAlSiO_4$	$NaLaF_4$+fluorite+LaF_3
800°C	$NaAlSiO_4$	fluorite+ LaF_3

To

The crystalline phases in glass and glass ceramics with 0% and 3% YbF_3

Heat treatment	YbF_3 content in the precursor glass (mol%)	
	0%	3%
-	amorphous	amorphous
500°C for 1 h	amorphous	$NaLaF_4$+fluorite
600°C for 1 h	$NaLaF_4$	$NaLaF_4$+fluorite
700°C for 1 h	$NaLaF_4$+$NaAlSiO_4$	$NaLaF_4$+fluorite+LaF_3
800°C for 1 h	$NaAlSiO_4$	fluorite+ LaF_3

The description of Fig. 4 changed from "SEM micrographs of glass (a,e) and glass ceramics doped with 1% ErF3 and 0% YbF3 (a-d) and 3% YbF3 (e-h) heat treated at b, f) 600-° C, c, d) 700° C and d, h) 800° C for 1 h" to "Fig. 4. SEM micrographs of glass and glass ceramics heat treated at 600-800° C for 1 h doped with (a-d) 0% YbF3 and (e-f) 3% YbF3." (page 9)

The temperatures of heat treatment are included in Fig. 4.

The contrast of Fig. 5 c) and f) is enhanced.

Error bars are included in inset of Fig. 7 a).

Standard errors are added to n values in Fig. 8.

“indicating three photon UCL (see Fig. 8 a).” replaced with “The absorption of n photons leads to power dependence of $I \propto P^n$ only in cases of infinitely small upconversion rates. The value of slopes can range from n to 1 (for upper excited states) or 0.5 (for intermediate states) [38]. At least three photon excitation is required for the population of 4G11/2 and 2H9/2, therefore contribution from two photon UCL can be excluded. The determined values of slopes are close to 2 due to relatively large UCL rates that reduce the values of the slopes [38].” (page 13, line 6-11).

“originate” replaced with “originates” (page 13, line 15).

“Three polymorphic modifications are known for LaOF: high temperature fluorite type α-LaOF (Fm m) and two distorted fluorite phases – rhombohedral β-LaOF (R m) and tetragonal γ-LaOF (P4/nmm) [24].” Replaced with “As mentioned previously, three polymorphic modifications (cubic, rhombohedral and tetragonal) of LaOF are known.” (page 17, line 6-7).

Error bars are added in the inset of Fig. 13.

*Abstract

Abstract

Novel Er^{3+} and Yb^{3+} doped transparent oxyfluoride glass ceramics containing $NaLaF_4$ nanocrystals were prepared from oxyfluoride glasses with general composition of Na_2O-NaF-LaF_3-Al_2O_3-SiO_2. The crystallization processes, changes in morphology and upconversion luminescence were analyzed. The heat treatment of the precursor glasses promoted the formation of hexagonal $NaLaF_4$ and an unidentified fluorite type compound. An enhancement of upconversion luminescence with the introduction of YbF_3 in the glass ceramics was detected and indicated an efficient energy transfer from Yb^{3+} to Er^{3+}. The local environment of Er^{3+} in hexagonal $NaLaF_4$ and the fluorite phase was analyzed using site-selective spectroscopy and compared with polycrystalline ceramics. The incorporation of Er^{3+} ions in three non-equivalent cationic sites in the crystalline lattice of hexagonal $NaLaF_4$ nanocrystals was observed. The local environment of erbium ions in the fluorite phase was found to be similar to α-$NaYF_4$ suggesting the formation of Er^{3+} and Yb^{3+} stabilized α-$NaLaF_4$.

Highlights (for review)

- New glass ceramics containing Er^{3+} and Yb^{3+} doped $NaLaF_4$ were prepared.
- The effect of introduction of YbF_3 in glass ceramics was analyzed.
- The dominant mechanisms of upconversion luminescence were investigated.
- The formation of fluorite type phase in phase-separated glass ceramics was discussed.

Upconversion luminescence of Er^{3+}/Yb^{3+} and their role in the stabilization of cubic $NaLaF_4$ nanocrystals in transparent oxyfluoride glass ceramics

Guna Krieke, Anatolijs Sarakovskis, Maris Springis

Institute of Solid State Physics, University of Latvia, 8 Kengaraga str., LV-1063, Riga, Latvia.

KEYWORDS: upconversion, site-selective spectroscopy**,** $NaLaF_4$, oxyfluoride, glass ceramics

Introduction

Transparent rare earth (RE) doped oxyfluoride glass ceramics are excellent composites for photonics applications, which combine the good chemical and mechanical properties of oxide glasses with the low phonon energy environment of fluoride crystals. In these materials RE ions are mostly incorporated in the crystalline phase, as the result the optical properties of oxyfluoride glass ceramics are comparable to fluoride crystals [1–3]. The low phonon energy of fluorides reduce the non-radiative transition probabilities and improve the efficiency of radiative transitions. It is especially important for upconversion luminescence (UCL) - an anti-Stokes process in which low energy photons are converted to photons of higher energy [4]. Efficient near infrared to visible UCL can be realized in Er^{3+} doped materials due to ladder-like energy level structure and long lifetimes of the emitting states. Yb^{3+} is often used as a sensitizer for Er^{3+} containing systems because it has a relatively large absorption cross-section of near-infrared transition resonant with transitions of Er^{3+} ions enabling efficient energy transfer from Yb^{3+} to Er^{3+} [5,6]. The UCL efficiency depends on the matrix, in which the RE ions are introduced. Highly efficient UCL has been observed in a family of $NaREF_4$ compounds, where RE: Y, Gd, La or Lu [7–10]. Two polymorphic modifications of these compounds are known - low temperature hexagonal β-$NaREF_4$ (for all RE) and high temperature fluorite type α-phase with chemical composition often expressed as $NaREF_4$ (for all RE except for La and Ce). In glass ceramics crystallization of hexagonal $NaLaF_4$ [11,12], β-$NaGdF_4$ [13,14] and β-$NaYF_4$ [15,16] as well as cubic phases such as $NaYF_4$ [17–19], $NaGdF_4$ [13,14], $NaYbF_4$ [20] and $NaLuF_4$ [21,22] has been observed. The UCL efficiency of cubic polymorphs are estimated to be two orders of magnitude lower than hexagonal phases, therefore the crystallization of the low temperature phase is favorable [8], however in glass

ceramics the formation of high temperature fluorite type compounds are often detected [1]. Among other fluorides, hexagonal $NaLaF_4$ is a perspective host for RE ions due to low average phonon energy (290 cm^{-1} [7]) and the absence of high temperature phases [23]. Up to now there are no reports about UCL processes in $NaLaF_4$ containing glass ceramics.

In this research, crystallization, UCL and local environment of Er^{3+} ions in Er^{3+} and Yb^{3+} doped transparent glass ceramics containing $NaLaF_4$ nanocrystals are analyzed. The effect of YbF_3 content on the phase formation and luminescence is discussed.

Materials and methods

Oxyfluoride glasses with general compositions of $19Na_2O$-3NaF-$5LaF_3$-$6Al_2O_3$-$67SiO_2$ doped with 1% ErF_3 and 0-3% YbF_3 (in mol%) were prepared from analytical grade raw materials by melt quenching. The mixtures of 10 g were melted in covered corundum crucibles at 1500^0C for 30 min. The resulting oxyfluoride melts were casted in stainless steel molds. The glass ceramics were obtained after isothermal heat treatment of the precursor glasses at the temperature range of 500-800^0C for 1 h. For identification of the crystalline phases in the glass ceramics, polycrystalline Er^{3+} doped LaF_3, hexagonal $NaLaF_4$, α-$NaYF_4$ and LaOF were prepared. Polycrystalline LaF_3, hexagonal $NaLaF_4$ and cubic non-stoichiometric α-$NaYF_4$ doped with 1 mol% ErF_3 were prepared using solid state synthesis. An appropriate amount of NaF and REF_3 were mixed in agate mortar, heat treated at 150^0C for 1 h in He/F_2 gas flow (90% He; 10% F_2) followed by the annealing at 700^0C for 1 h in Ar atmosphere. Single phase polycrystalline cubic, tetragonal and rhombohedral LaOF doped with 1 mol% ErF_3 were prepared by the decomposition of (La,Er)F(CO_3) using procedure described in [24]. An alteration was made for the cubic polymorph – the heat treatment of (La,Er)F(CO_3) was carried at 800^0C for 10 min under argon protection followed by quenching in water to prevent phase transition from cubic to tetragonal and rhombohedral LaOF.

DTA measurements were carried out using Shimadzu Corp. DTG-60 with the heating rate of 10 K/min under an argon flow and using α-Al_2O_3 as a reference material with ±1°C precision. X-ray diffraction (XRD) measurements were performed with X-ray diffractometer PANalytical X'Pert Pro, using Cu tube (K_α radiation) operated at 40 kV and 30 mA. The unit cell parameters were calculated using DICVOL06 [25] and Fullprof software [26]. The standard uncertainties were calculated using inverted least-squares matrix assuming the

absolute error of each line to be 0.03 2θ (degree). The microstructures of glass ceramics were characterized by scanning electron microscopy (SEM) Tescan Lyra operated at 15 kV and transmission electron microscopy (TEM) with Tecnai G2 F20 operated at 200 kV. For SEM measurements, fractured, uncoated surfaces were used. The UCL in different experiments was excited by either a pulsed wavelength-tunable solid state laser Ekspla NT342/3UV (pulse duration – 4 ns, linewidth 4.3 cm^{-1}) or a temperature controlled laser diode (λ_{em}= 975 nm, variable radiant power up to 1 W). The luminescence spectra were measured by Andor DU-401-BV CCD camera coupled to Andor SR-303i-B spectrometer. The power dependence of UCL intensity was fitted to power function using a minimum chi-square estimation. Slopes of log-log plots were determined for low power region (20-400 mW) with coefficient of determination R^2 better than 0.998. Luminescence decay times were measured by a photomultiplier tube (time resolution better than 20 ns) and digital oscilloscope Tektronix TDS 684A. Effective luminescence decay time was calculated as weighted average [27] with standard error calculated assuming exponential distribution. For low temperature measurements, the samples were mounted on a cold finger type He cryostat (Advanced Research Systems DE202 N).

Results and discussion

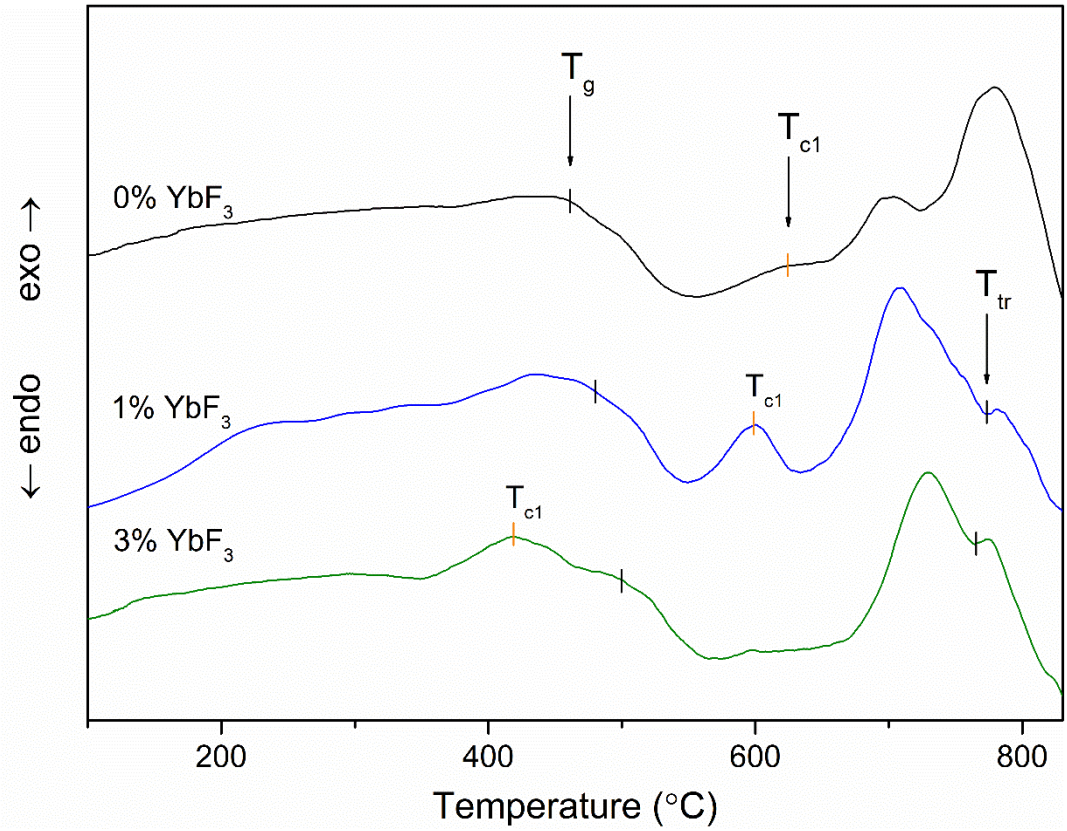

Fig. 1. DTA curves of glasses doped with 1% ErF_3 and 0, 1 and 3% YbF_3.

Fig. 1 shows the DTA curves of the glasses with 0, 1 and 3% YbF_3. The characteristic temperatures are summarized in the Table 1.

Table 1

Thermal properties of oxyfluoride glasses

YbF_3 (mol%)	T_g (°C)	T_{c1} (°C)	T_{tr} (°C)
0%	460±1	630±1	-
1%	480±1	600±1	765±1
3%	500±1	420±1	760±1

The glass transition temperature T_g is located at approximately 460-500^{0}C and it increases for the glasses with higher YbF_3 content, which is rather unusual behavior considering that the introduction of glass modifier should lead to a decrease of the connectivity of glass network and result in the reduction of the T_g. Unexpected changes can also be observed for the exothermic effect T_{c1} associated with the crystallization of fluoride nanocrystals. For the glass ceramics with 0% YbF_3 a broad exothermic effect is detected with a maximum at around 630^{0}C, however the characteristic temperature is considerably reduced with the increase of YbF_3 content in the glass. For the glass ceramics with 3% of YbF_3 this exothermic effect can be observed at ~420^{0}C - a temperature lower than T_g. Both the increase of the glass transition temperature and decrease of the T_{c1} below T_g with the introduction of YbF_3 suggest the phase separation. Immiscibility is characteristic to halide containing silicate melts [28], and phase separation has been detected in several oxyfluoride glasses [13,22,29,30]. In a systematic investigation of the phase separated oxyfluoride melts it was observed that alkali and RE ions are mostly incorporated in the fluoride-rich phase [30,31]. In the present study the introduction of a high amount of YbF_3 increases the fluorine content in the melt and it should enhance the immiscibility of silicate melt and fluoride phase enriched in Na^+ and RE^{3+} ions. As the result the base glass should be depleted in glass modifiers (Na^+ and RE^{3+}), therefore the glass transition temperature of this phase should increase. In phase separated glasses two or more glass transition temperatures are expected. Unfortunately, in the investigated glasses, no second T_g, corresponding to the glass transition temperature of the fluoride-rich phase could be detected, nevertheless phase separation was detected in TEM analysis discussed further in the text.

The additional exothermic effects located at temperature above 700^{0}C can be ascribed to several processes. According to the XRD data (see Fig. 3.) for the glass ceramics with 0% YbF_3 these effects are associated mainly with the surface crystallization of aluminosilicates, however, in the glasses with higher YbF_3 content, crystallization of LaF_3 is observed.

An endothermic effect T_{tr} located at ~770^{0}C is in a good agreement with the incongruent melting temperature of hexagonal $NaLaF_4$ (787^{0}C) [32]. The exact melting temperature remains unknown due to partial overlapping with the exothermic effects. T_{tr} is not observed

for the glass with 0% YbF_3 probably due to the low content of $NaLaF_4$ in the glass ceramics (see Fig.2).

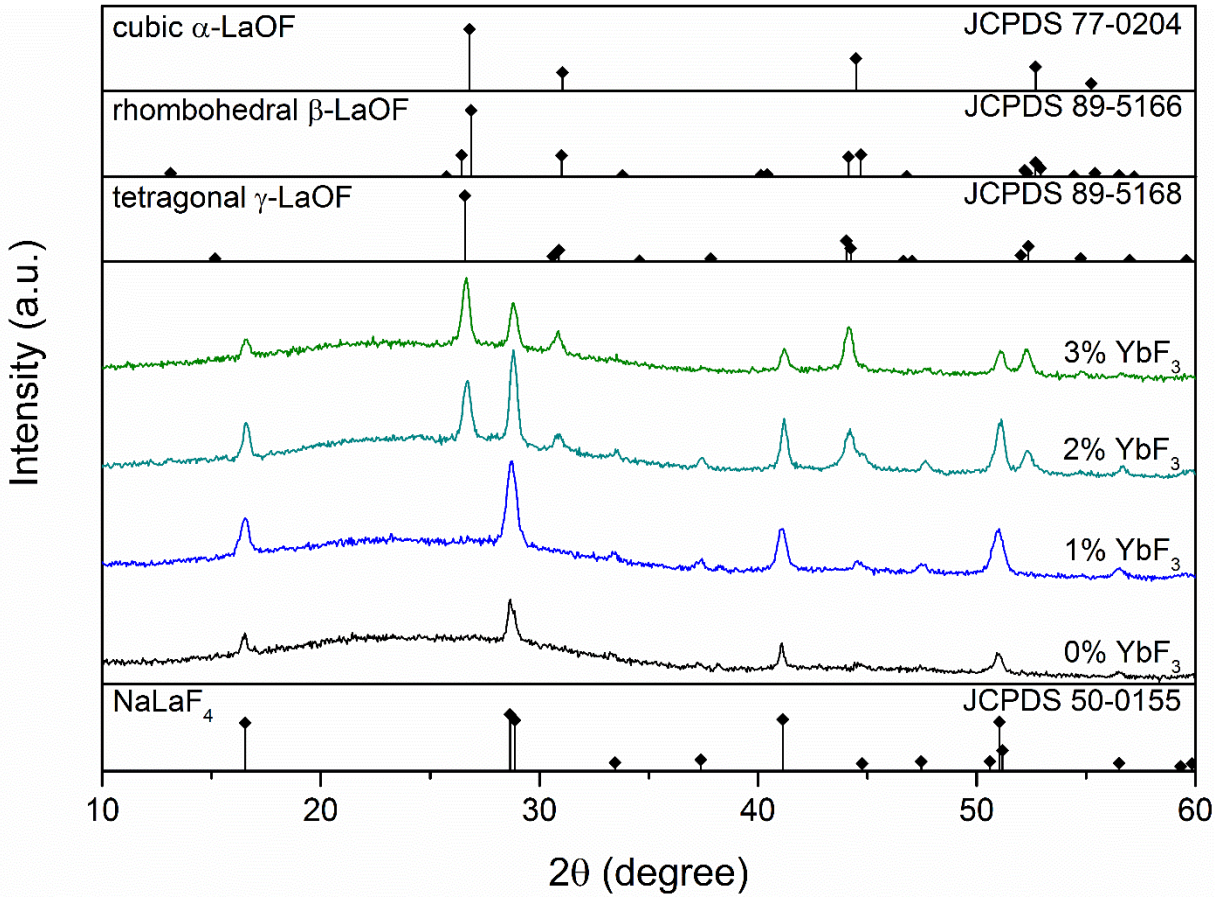

Fig. 2. XRD patterns of glass ceramics heat treated at 600^0C for 1 h.

The glasses annealed at 600^0C for 1 h show XRD peaks, which are attributed to hexagonal $NaLaF_4$ (see Fig. 2). However, in the glass ceramics with YbF_3 content higher than 1% another crystalline compound is present. It is a fluorite type compound seemingly isostructural with cubic LaOF having a unit cell parameter a=5.782±0.006 Å. Three polymorphic modifications are known for LaOF: high temperature fluorite type α-LaOF ($Fm\bar{3}m$) and two distorted fluorite phases – rhombohedral β-LaOF ($R\bar{3}m$) and tetragonal γ-LaOF ($P4/nmm$) [24]. Due to similarities in the crystalline structure of fluorite and distorted fluorite phases, all three modifications agree reasonably well with the XRD pattern. An isostructural crystalline compound has been observed in other glass ceramics [33,34] and the authors identify it as a rhombohedral LaOF based on XRD data despite the absence of the superstructure peaks characteristic to the rhombohedral distortion in fluorite lattice. However,

it is often difficult to observe superstructure peaks of related structures especially in nanocrystalline glass ceramics, therefore the identification of such phases should not be based only on XRD data. The formation of LaOF in fluorine enriched glasses is questionable because La^{3+} ions have strong affinity for fluorine ions in oxyfluorides [35]. The relative intensity of this fluorite type compound increases with the increase of YbF_3, which is highly unusual because the relative fluorine content in the glass is increased with the introduction of YbF_3. The origin of the fluorite type compound in the investigated glass ceramics will be analyzed using luminescence measurements (site-selective spectroscopy) and will be discussed further in the text.

The effect of the heat treatment temperature on the phase formation in glass ceramics doped with 0% YbF_3 (containing only hexagonal $NaLaF_4$) and 3% YbF_3 (containing a mixture of hexagonal $NaLaF_4$ and cubic fluorite type compound) was analysed in details.

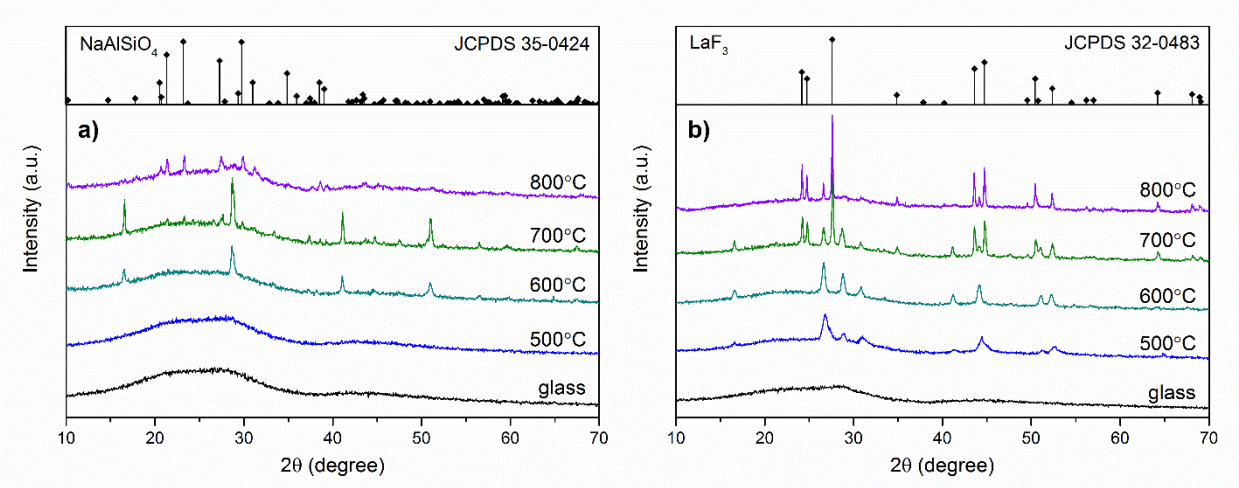

Fig. 3. XRD patterns of glasses and glass ceramics heat treated at different temperatures for 1 h doped with a) 0% YbF_3 and b) 3% YbF_3.

Fig. 3. a shows the XRD patterns of precursor glass and glass ceramics doped with 0% YbF_3 heat treated at 500-800^{0}C for 1 h. No sharp diffraction peaks can be detected for glass and glass ceramics heat treated at 500^{0}C indicating an amorphous structure. After heat treatment at 600^{0}C, intense diffraction peaks ascribed to hexagonal $NaLaF_4$ are observed. The heat treatment at 700^{0}C for 1 h promoted the growth of $NaLaF_4$ nanocrystals – the XRD peaks became more intense and narrow. Several additional low intensity peaks can be assigned to

aluminosilicate nepheline. After the increase of the temperature of heat treatment up to 800^{0}C only nepheline is present in the sample and no fluoride phases can be detected. As mentioned previously hexagonal $NaLaF_4$ is stable up to 787^{0}C, as the result, the heat treatment at higher temperature prevents the formation of this compound in the investigated glass ceramics.

More complex processes are observed in the glass ceramics with higher YbF_3 content. The XRD patterns of precursor glass and glass ceramics with 3% YbF_3 are shown in Fig. 3. b. The precursor glass is amorphous. The heat treatment close to T_{c1} (500^{0}C) results in a formation of a mixture of $NaLaF_4$ and the fluorite type compound isostructural with α-LaOF. The increase of the heat treatment up to 700^{0}C improves the crystallinity of these compounds, however several new diffraction peaks assigned to LaF_3 are present in the XRD pattern of the glass ceramics heat treated at 700^{0}C. There is also a considerable peak shift to lower angles for the fluorite type compound with the increase of the heat treatment suggesting incorporation of the ions with larger ionic radii in the cubic lattice. The ionic radii of La^{3+}, Er^{3+} and Yb^{3+} for eight-fold coordination characteristic to RE ions in fluorite structure [36] are 1.160, 1.004 and 0.985 Å [37] respectively, therefore the changes in the lattice parameters can be explained by the incorporation of La^{3+} in the fluorite nanocrystals containing Er^{3+} and Yb^{3+}.

Similar to the glass ceramics with 0% YbF_3, the presence of $NaLaF_4$ cannot be detected after the heat treatment at 800^{0}C, however both fluorite type phase and LaF_3 are present in the glass ceramics.

The phase formation in glass ceramics with 0% and 3% YbF_3 are summarized in Table 2.

Table 2.

The crystalline phases in glass and glass ceramics with 0% and 3% YbF_3

Heat treatment	YbF_3 content in the precursor glass (mol%)	
	0%	3%
-	amorphous	amorphous
500°C for 1 h	amorphous	$NaLaF_4$+fluorite
600°C for 1 h	$NaLaF_4$	$NaLaF_4$+fluorite

700°C for 1 h	$NaLaF_4$+$NaAlSiO_4$	$NaLaF_4$+fluorite+LaF_3
800°C for 1 h	$NaAlSiO_4$	fluorite+ LaF_3

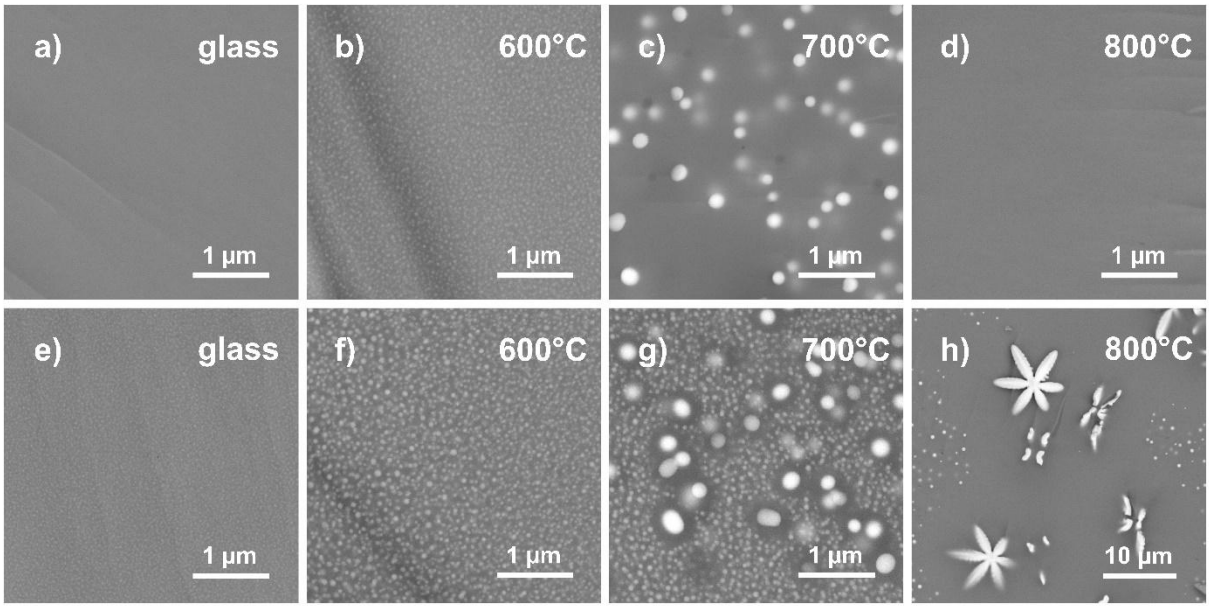

Fig. 4. SEM micrographs of glass and glass ceramics heat treated at 600-800°C for 1 h doped with (a-d) 0% YbF_3 and (e-f) 3% YbF_3.

SEM micrographs of fractured surfaces of glass and glass ceramics with 0% YbF_3 and 3% YbF_3 are presented in Fig. 4. In the glass with 0% YbF_3 (Fig. 4. a) no presence of secondary phases can be observed, however, after heat treatment at 600-700^{0}C (Fig. 4. c, d) for 1 h spherical homogeneously dispersed particles are formed. The lighter sections represent particles enriched in heavier elements (such as RE) dispersed in glass matrix (darker sections) containing lighter elements. In this sample the spherical particles are assumed to be hexagonal $NaLaF_4$ nanocrystals and it is a typical morphology of fluorides in many oxyfluoride glass ceramics [16,22,27]. It should be noted that the increase of the temperature of heat treatment from 600 to 700^{0}C leads to a formation of larger crystals, however the number of crystallites is considerably lower suggesting a decrease of nucleation rate at higher temperature. After heat treatment at 800^{0}C for 1 h the morphology of the glass ceramics strongly resembles amorphous glass (except for small scale surface crystallization of aluminosilicates not shown in the micrographs). The results are in a good agreement with XRD data (see Fig. 3.) and

suggest that the formation of $NaLaF_4$ is prevented in glass ceramics at temperature above the incongruent melting point of this compound.

Considerably different processes can be observed in the glass ceramics with 3% YbF_3 (Fig. 4. e-h). In the precursor glass fine hardly detectable regions enriched in heavy elements are present suggesting a phase separation during the cooling of the melt. The thermal treatment promotes the growth of these particles, but, similar to glass ceramics with 0% YbF_3 the number of the crystallites is reduced. In this case a nucleation rate would have insignificant impact on the crystallization of these fluorides due to the presence of nucleation centers in the precursor glass. A probable explanation is Ostwald ripening – a dissolution of smaller particles in the glass matrix enabling the coarsening of the larger crystals. The size of the crystals is even further increased after the heat treatment at 800^0C for 1 h (Fig. 4. h). Large hexagonal dendrites up to 10 μm identified as LaF_3 are formed in the glass, suggesting major decrease of the glass viscosity. Such changes in the morphology lead to considerable light scattering (see Fig. 6).

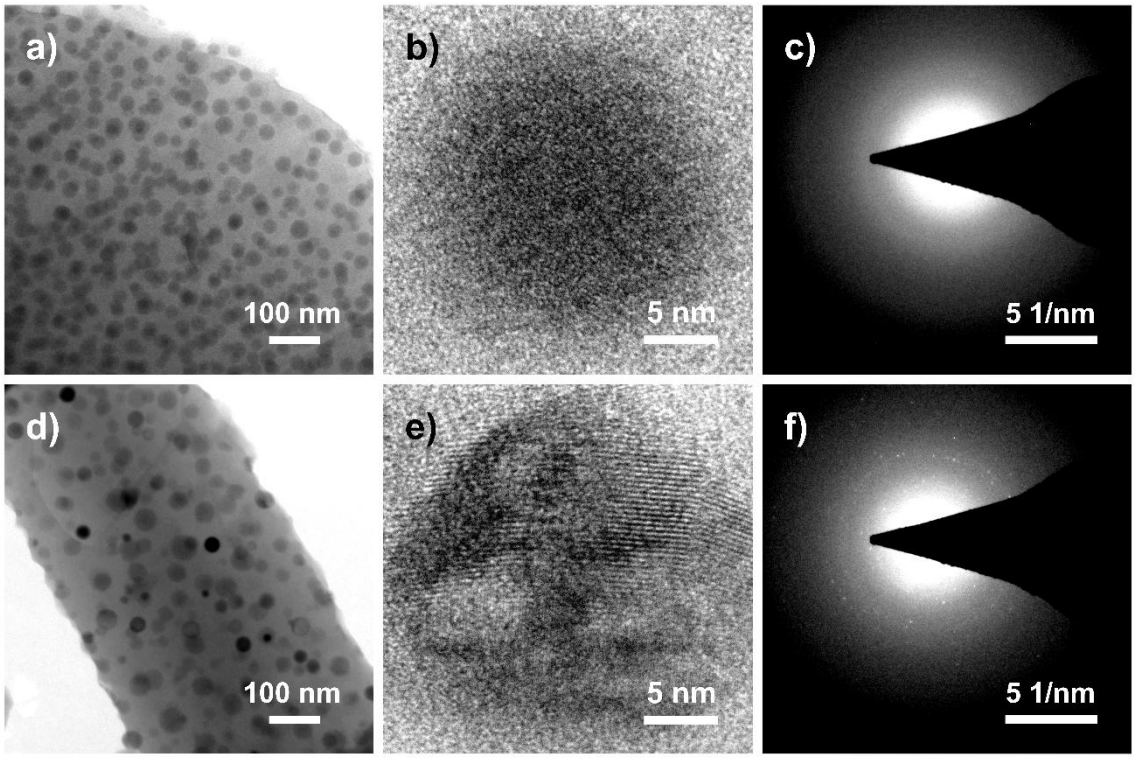

Fig. 5. TEM micrographs and selected area diffraction patterns of a-c) glass and d-f) glass ceramics doped with 3% YbF_3 heat treated at 600^0C for 1 h.

TEM micrographs for the glass and glass ceramics doped with 3% YbF_3 are shown in Fig. 5. In both glass and glass ceramics spherical particles (darker sections) are homogeneously distributed in the glass matrix (lighter regions). In the glass sample no long-range order can be detected in the particles and the selected area diffraction pattern shows broad halo characteristic to an amorphous structure, indicating a phase separation during the cooling of the melt (see Fig. 5. b and c). The heat treatment promotes the formation of polycrystalline particles, presumably hexagonal $NaLaF_4$, and the fluorite phase. No considerable changes in the average size of these particles (36±7 nm) can be detected in comparison to the base glass, therefore we assume that the phase separation droplets in these materials act a nucleating agent – the nanocrystals are formed in the fluorine-rich regions. These results are in a good agreement with the DTA data (see Fig. 1.). Due to the phase separation exothermic effect ascribed to the crystallization of fluoride nanocrystals, can be detected at temperature lower than T_g.

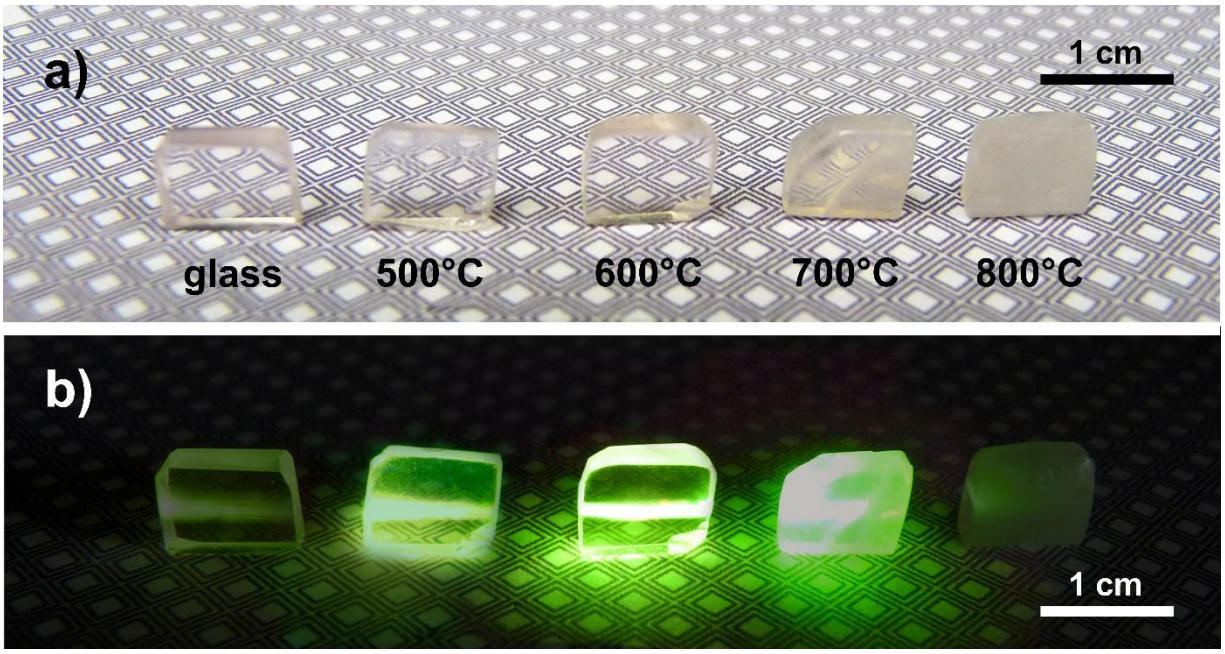

Fig. 6. Photographs of the glass and glass ceramics doped with 2% YbF_3 a) as prepared and b) excited at 975 nm.

The photographs of glass and glass ceramics doped with 2% YbF_3 heat treated at different temperatures are shown in Fig. 6. Due to the small size of nanocrystals, highly transparent samples can be obtained after heat treatment up to 600^0C for 1 h. According to SEM

characterization (see Fig. 4.), the scattering in the glass ceramics prepared at higher temperature is caused by the formation of large fluoride crystals.

In the glass ceramics efficient UCL is observed. The highest intensity of UCL was detected for the glass ceramics heat treated at 600-700^{0}C for 1 h. The samples heat treated at 600^{0}C for 1 h exhibit both efficient UCL and excellent transparency, therefore these materials were chosen for further detailed spectroscopic characterization.

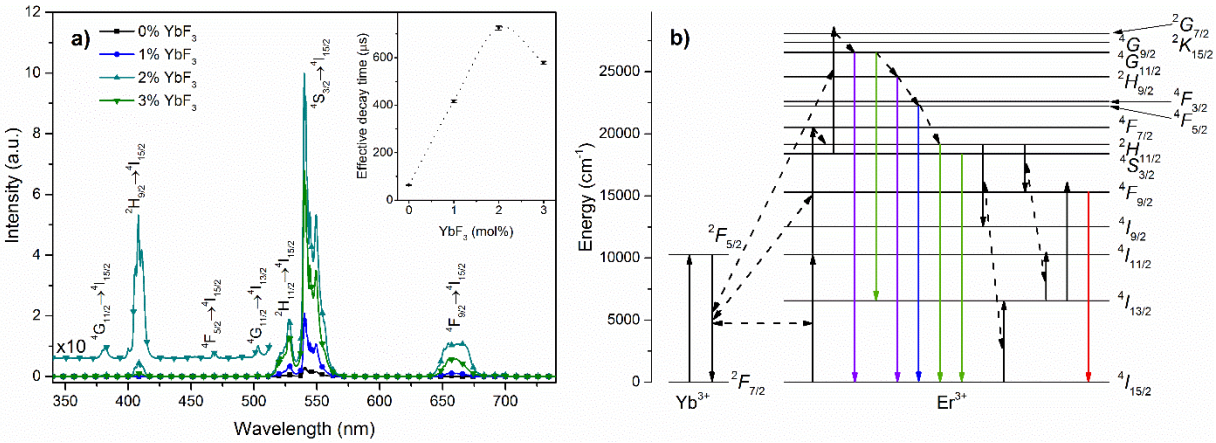

Fig. 7. a) UCL spectra of Er^{3+} ions in the glass ceramics with 1% ErF_3 and 0-3% YbF_3 heat treated at 600^{0}C for 1 h excited at 978 nm. Inset: The dependence of UCL green emission decay time on the YbF_3 content in glass ceramics. b) Partial energy level scheme of Er^{3+} and Yb^{3+} and the possible UCL mechanisms.

The UCL spectra of the Er^{3+} ions in glass ceramics are shown in Fig. 7. a. The most intense luminescence bands can be assigned to $^2H_{11/2}\rightarrow{}^4I_{15/2}$ (520 nm), $^4S_{3/2}\rightarrow{}^4I_{15/2}$ (540 nm) and $^4F_{9/2}\rightarrow{}^4I_{15/2}$ (660 nm) transitions of Er^{3+} ions. Several additional luminescence bands ascribed to three photon UCL originate from transitions of $^4G_{11/2}$, $^2H_{9/2}$ and $^4F_{5/2}$ excited states. When YbF_3 was introduced in the glass ceramics, considerable enhancement of UCL was observed. The highest intensity of UCL was detected for the glass ceramics with 2% YbF_3. The decrease of luminescence decay time (see inset of Fig. 7. a) and UCL intensity of the glass ceramics with 3% YbF_3 suggest an appearance of additional non-radiative de-excitation pathway that reduces the efficiency of the UCL.

The intensity of UCL emission is proportional to the n-th power of excitation power, where n is the number photons required to excite the emitting states assuming small upconversion rates

[38]. The pumping power dependence of UCL intensity of the most intense UCL emission bands was investigated for the glass ceramics with highest UCL efficiency (2% YbF_3) (see Fig. 8.).

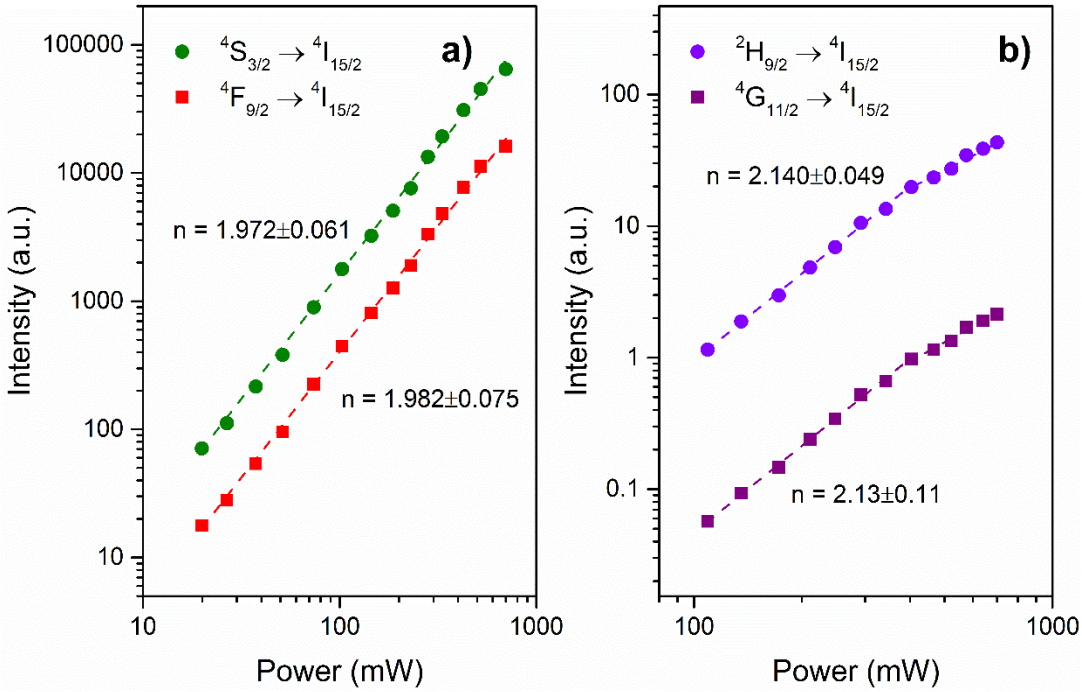

Fig. 8. Power dependence of UCL intensity of a) $^4S_{3/2} \rightarrow {}^4I_{15/2}$ (green), $^4F_{9/2} \rightarrow {}^4I_{15/2}$ (red) and b) $^2H_{9/2} \rightarrow {}^4I_{15/2}$ (violet), $^4G_{11/2} \rightarrow {}^4I_{15/2}$ (ultraviolet) emission in the glass ceramics with 2% YbF_3.

For the green and red emission, the slopes of the log–log pump power dependences (n=1.97-1.98) are close to 2, suggesting two photon UCL (see Fig. 8 a). However, higher values (n=2.13-2.14) in the low power region are detected for violet ($^2H_{9/2} \rightarrow {}^4I_{15/2}$) and ultraviolet ($^4G_{11/2} \rightarrow {}^4I_{15/2}$) emission (see Fig. 8 a). The absorption of n photons leads to power dependence of $I \propto P^n$ only in cases of infinitely small upconversion rates. The value of slopes can range from n to 1 (for upper excited states) or 0.5 (for intermediate states) [38]. At least three photon excitation is required for the population of $^4G_{11/2}$ and $^2H_{9/2}$, therefore contribution from two photon UCL can be excluded. The determined values of slopes are close to 2 due to relatively large UCL rates that reduce the values of the slopes [38]. The possible UCL mechanisms are summarized in Fig. 7. b. For the glass ceramics with 0% YbF_3 the electrons are excited from $^4I_{15/2}$ to $^4I_{11/2}$ by absorption of a near infrared photon. Afterwards they are excited to $^4F_{7/2}$ by excited state absorption or energy transfer between Er^{3+} ions. A rapid multiphonon de-

excitation form $^4F_{7/2}$ populate $^2H_{11/2}$ and $^4S_{3/2}$ emitting states from which the green emission originates. The absorption of the third infrared photon results in the excitation of $^2G_{7/2}$ from which rapid non-radiative multiphonon relaxation populates $^4G_{11/2}$, $^2H_{9/2}$ and $^4F_{5/2}$ excited states. As the result, ultraviolet, violet and blue UCL emerge, however, the intensity of these luminescence bands are considerably lower in comparison to the two photon UCL. The non-radiative multiphonon relaxation from $^4S_{3/2}$ to $^4F_{9/2}$ is not efficient in low-phonon hosts such as $NaREF_4$ [15], however this energy level can be populated by cross-relaxation ($^2H_{11/2}$,$^4I_{15/2}$→$^4I_{9/2}$,$^4I_{13/2}$ followed by $^2H_{11/2}$,$^4I_{13/2}$→$^4F_{9/2}$,$^4I_{11/2}$), excited state absorption or energy transfer from $^4I_{13/2}$ to $^4F_{9/2}$. The increase of the effective luminescence decay time (see inset of Fig. 7. a) suggests that for YbF_3 containing glass ceramics energy transfer from Yb^{3+} to Er^{3+} is the dominant mechanism of UCL. The decrease of the UCL efficiency for glass ceramics with 3% YbF_3 can be explained by energy back-transfer from Er^{3+} to Yb^{3+}.

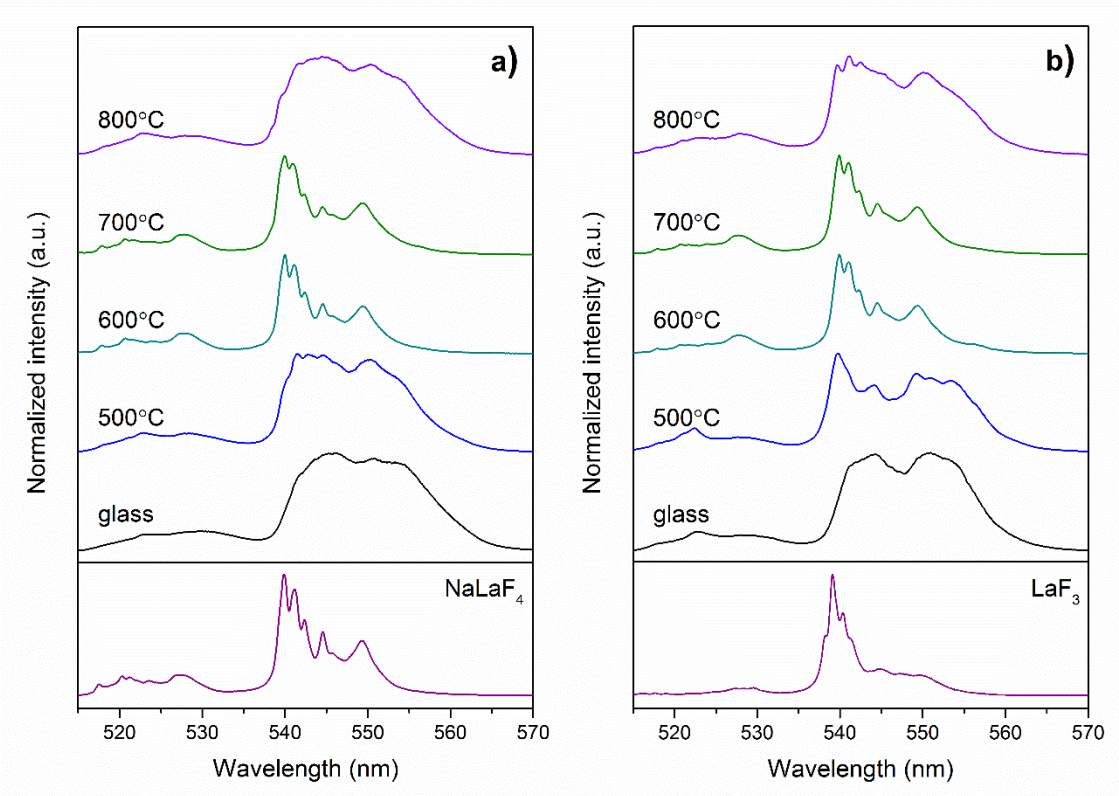

Fig. 9. UCL spectra of Er^{3+} green emission excited at 978 nm of glass and glass ceramics heat treated at 500-800^{0}C for 1 h doped with 1% ErF_3 and a) 0% YbF_3 and b) 3% YbF_3. Lower section: upconversion luminescence spectra of erbium doped polycrystalline $NaLaF_4$ and LaF_3 excited at 978 nm.

Fig. 9. a shows the comparison of the UCL spectra for Er^{3+} green emission in glass and glass ceramics with 0% YbF_3 heat treated at 500-800^{0}C for 1 h. The luminescence spectra of the glass and glass ceramics heat treated at 500^{0}C and 800^{0}C exhibit broad luminescence bands characteristic to Er^{3+} ions in amorphous environment. The precursor glass and glass ceramics heat treated at 500^{0}C are amorphous (see Fig. 3. a), however the glass ceramics heat treated at 800^{0}C contain aluminosilicates. The absence of narrow, resolved luminescence bands characteristic to Er^{3+} ions in crystalline environment suggest that the Er^{3+} ions are mainly incorporated in the amorphous matrix. The luminescence spectra of the glass ceramics heat treated at 600-700^{0}C closely resemble polycrystalline $NaLaF_4$ indicating that the UCL emission in these glass ceramics originate from Er^{3+} ions in the hexagonal $NaLaF_4$ nanocrystals.

The luminescence spectrum of the precursor glass with 3% YbF_3 does not contain any sharp peaks suggesting that the Er^{3+} ions are located in amorphous environment. New features appearing in the luminescence spectrum of the glass ceramics treated at 500^{0}C suggest the incorporation of Er^{3+} ions in the nanocrystals, however the luminescence spectrum differs from Er^{3+} doped $NaLaF_4$. According to the XRD data (see Fig. 3. b) the glass ceramics heat treated at 500°C for 1 h mostly contains fluorite type compound, therefore we assume that this luminescence spectrum is characteristic to the Er^{3+} ions incorporated in the fluorite-type nanocrystals. In the temperature range 600-700^{0}C the luminescence spectra resemble hexagonal $NaLaF_4$, however at 800^{0}C it is similar to the amorphous glass suggesting that Er^{3+} instead of incorporating in the hexagonal dendrites of LaF_3 (see Fig. 4) remain mostly in the glass matrix.

The glass ceramics with 0% and 3% YbF_3 were analyzed in details using time-resolved site-selective spectroscopy. At low temperatures, different local environment of Er^{3+} ions can be selectively excited. As the result Er^{3+} ions in different local environment can be detected and distinguished by luminescence and luminescence excitation spectra.

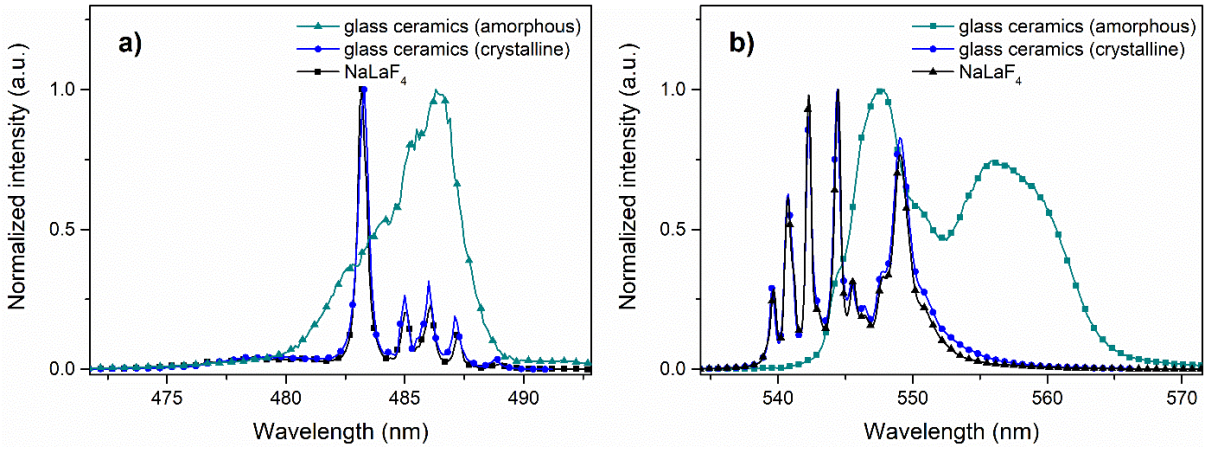

Fig. 10. a) excitation spectra (exciting $^4F_{7/2}$, detecting green emission) and b) the green emission spectra (excited at 486 nm) of Er^{3+} ions in the glass ceramics with 1% ErF_3 and 0% YbF_3 heat treated at 600^{0}C for 1 h compared with the polycrystalline $NaLaF_4$ measured at 10 K.

In the glass ceramics with 0% YbF_3 two different luminescence excitation and luminescence spectra of green emission can be detected (see Fig. 10.). One exhibits broad featureless luminescence and luminescence excitation bands characteristic to Er^{3+} ions in amorphous environment and the other is similar to the polycrystalline $NaLaF_4$. The results suggest that Er^{3+} ions in the glass ceramics are located in both crystalline phase (hexagonal $NaLaF_4$) and glass matrix.

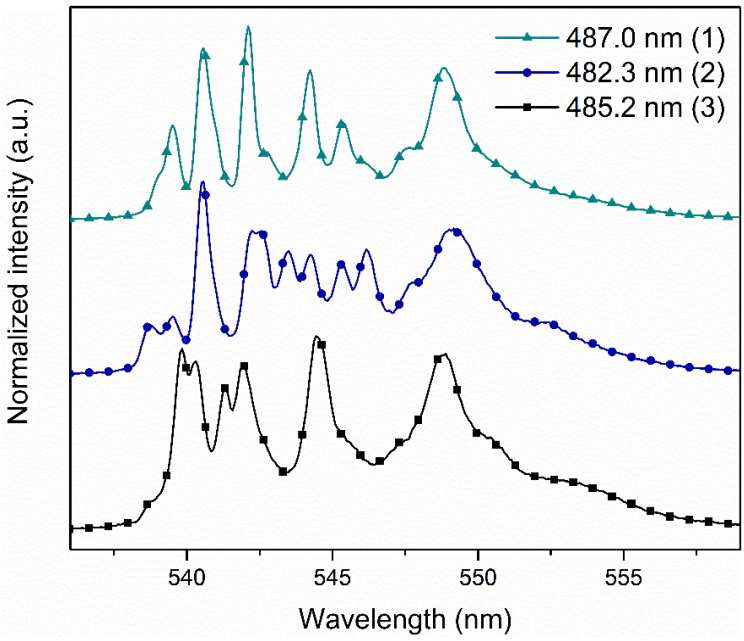

Fig. 11. Luminescence spectra of Er^{3+} ions in glass ceramics with 1% ErF_3 and 0% YbF_3 heat treated at 600^{0}C for 1 h detected at 10 K.

In addition, three distinct spectra of Er^{3+} ions in the crystalline environment could be detected (see Fig. 11). In the crystalline lattice of $NaREF_4$ there are three cationic position: the first site occupied by RE^{3+} ions, the second by alternating Na^+ and RE^{3+} ions with ratio 1:1 and the third half occupied by Na^+ ions [39]. It is reasonable to assume that Er^{3+} ions in the $NaLaF_4$ lattice would efficiently replace La^{3+} and incorporate in the first two cationic sites. In these glass ceramics the existence of three distinct luminescence spectra suggests that Er^{3+} ions incorporate not only in the first two cationic sites, but may be localized also in third half occupied by Na^+ site. Similar results are reported for polycrystalline Er^{3+} doped $NaLaF_4$ [40].

In the glass ceramics doped with 3% YbF_3 site-selective spectroscopy was used to identify the fluorite phase isostructural with α-LaOF detected in these glass ceramics. For these measurements glass ceramics heat treated at 500^{0}C for 1 h was used to minimize impact from hexagonal $NaLaF_4$.

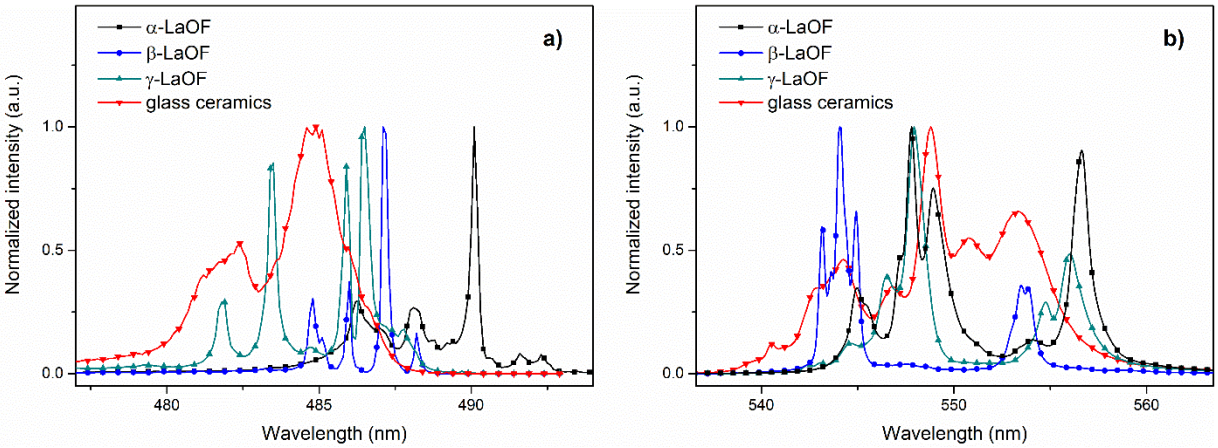

Fig. 12. a) Luminescence excitation spectra of Er^{3+} (exciting $^4F_{7/2}$, detecting green emission) in LaOF compared with the glass ceramics doped with 1% ErF_3 and 3% YbF_3 heat treated at 500°C for 1 h, monitoring green emission at 10 K and b) Luminescence spectra of Er^{3+} green emission in LaOF compared with the glass ceramics excited at the maximal intensity of each compound monitored at 10 K.

As mentioned previously, three polymorphic modifications (cubic, rhombohedral and tetragonal) of LaOF are known. The luminescence excitation (Fig. 12. a) and luminescence

spectra (Fig. 12. b) of Er^{3+} green emission of fluorite compound detected in glass ceramics were compared with all three modifications of LaOF. Considerable differences in the both clearly indicate that the local environment of Er^{3+} ions in the fluorite type phase is completely different from the three polymorphic modifications of LaOF. We can conclude that the cubic fluorite type nanocrystals detected in glass ceramics are not LaOF.

As mentioned previously, similar cubic compounds with general composition of $NaREF_4$ have been observed in most $NaF\text{-}REF_3$ binary systems except for LaF_3 and CeF_3. The $\alpha\text{-}NaREF_4$ is a non-stoichiometric compound where the $NaF\text{-}REF_3$ ratio can be varied. According to Ref. [23] the upper REF_3 limit is 64.3 mol% and lower ranges from 39 mol% (for $NaF\text{-}LuF_3$) to 55.5 mol% (for $NaF\text{-}PrF_3$), as the result the lattice parameter of these fluorite phases depends not only on the ionic radii of the RE ions, but also on the stoichiometry of these compounds.

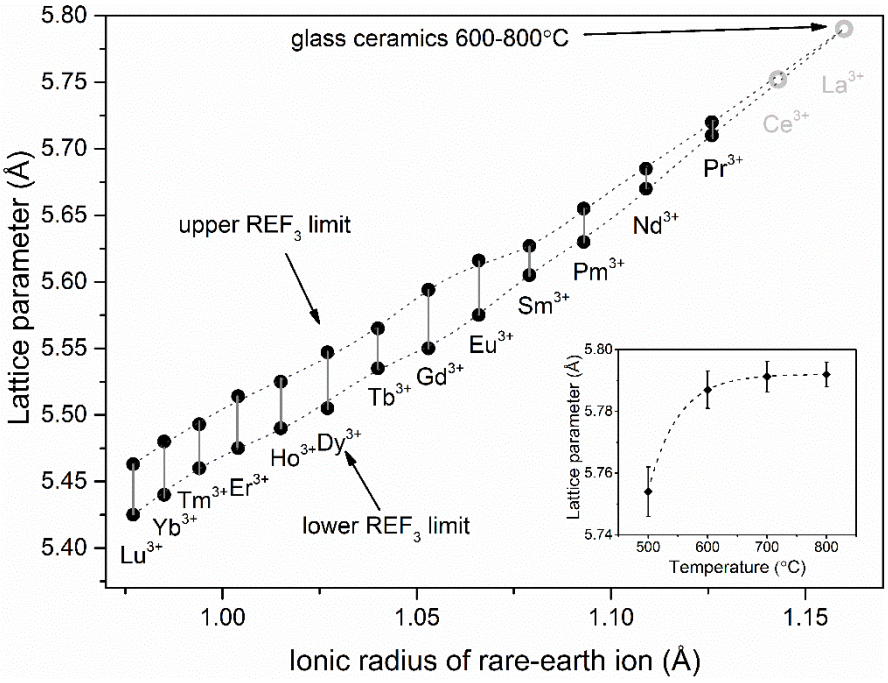

Fig. 13. Lattice parameter of $\alpha\text{-}NaREF_4$ phases with variable $NaF\text{-}REF_3$ ratio according to [23]. Ionic radii taken from [37]. Inset: lattice parameter of fluorite phase in glass ceramics heat treated at 500-600^{0}C for 1h.

Fig. 13. represents the variation of unit cell parameters of $\alpha\text{-}NaREF_4$. The lattice parameters of $NaCeF_4$ and $NaLaF_4$ can be extrapolated from the literature data, suggesting that for cubic NaLaF4 it would be 5.79 Å. It is in a good agreement with the lattice parameter of the fluorite

phase detected by XRD measurements, therefore we propose the formation of cubic $NaLaF_4$ in the glass ceramics. This assumption is in a good agreement with the XRD data (Fig. 2. and inset of Fig. 13.), which show a considerable increase of the lattice parameter of the fluorite compound with the increase of heat treatment (from 5.754 Å (500^0C for 1 h) to 5.787 Å (600^0C 1 h). This suggests that the smaller RE ions (Er^{3+}, Yb^{3+}) could act as nucleating agents and stabilize the cubic structure of α-$NaLaF_4$.

The structure of all α-$NaREF_4$ and thus the local symmetry of rare-earth activators in these compounds are analogous, therefore the luminescence spectra of different α-$NaREF_4$ should be similar. To confirm the formation of cubic $NaLaF_4$ in the investigated glass ceramics, we compared the low temperature spectra of the cubic compound prepared in glass ceramic with 3% YbF_3 heat treated at 500°C for 1 h with polycrystalline nonstoichiometric α-$NaYF_4$.

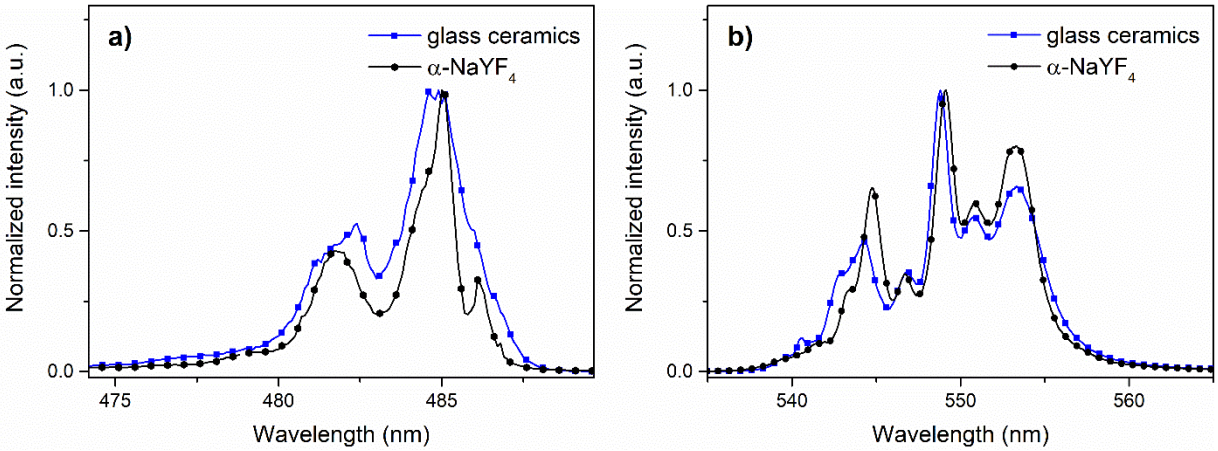

Fig. 14. a) Luminescence excitation spectra of Er^{3+} in α-$NaYF_4$ compared with the glass ceramics (3% YbF_3) heat treated at 500°C for 1 h, monitoring green emission at 10 K and b) luminescence spectra of Er^{3+} green emission in α-$NaYF_4$ compared with the glass ceramics monitored at 10 K.

The luminescence and luminescence excitation spectra are undoubtedly similar for the non-stoichiometric α-$NaYF_4$ and the cubic compound detected in glass ceramics with high YbF_3 content (see Fig. 14.) implying that the local symmetry of the Er^{3+} ions in these material are alike. The results confirm our hypothesis that the cubic face centered fluorite phase detected in these glass ceramics is in fact α-$NaLaF_4$ possibly stabilized by Yb^{3+} and Er^{3+}.

Conclusions

New transparent glass ceramics containing Er^{3+} and Yb^{3+} doped $NaLaF_4$ were prepared using melt quenching and heat treatment of precursor glasses. Efficient UCL was observed under near infrared excitation. In the glass ceramics with low YbF_3 content the formation of hexagonal $NaLaF_4$ and incorporation of Er^{3+} ions in three distinct cationic positions in the crystalline lattice was detected. However, the increase of YbF_3 content resulted in the formation of cubic phase isostructural with fluorite type LaOF. The detailed site selective spectroscopy and x-ray diffraction analysis of the crystallized glass ceramics suggest the formation of Yb^{3+} and Er^{3+} stabilized cubic α-$NaLaF_4$, for the first time obtained in oxyfluoride glass ceramics system.

Acknowledgments

The authors wish to express gratitude to K. Smits for TEM measurements. This work was supported by National Research Program $IMIS^2$ and Arnis Riekstins "MikroTik" donation. Donations are administered by the University of Latvia Foundation.

References

[1] P.P. Fedorov, A.A. Luginina, A.I. Popov, Transparent oxyfluoride glass ceramics, J. Fluor. Chem. 172 (2015) 22–50. doi:10.1016/j.jfluchem.2015.01.009.

[2] J. Qiu, Q. Jiao, D. Zhou, Z. Yang, Recent progress on upconversion luminescence enhancement in rare-earth doped transparent glass-ceramics, J. Rare Earths. 34 (2016) 341–367. doi:10.1016/S1002-0721(16)60034-0.

[3] M. Clara Gonçalves, L.F. Santos, R.M. Almeida, Rare-earth-doped transparent glass ceramics, Comptes Rendus Chim. 5 (2002) 845–854. doi:10.1016/S1631-0748(02)01457-1.

[4] F. Auzel, Upconversion and Anti-Stokes Processes with f and d Ions in Solids, Chem. Rev. 104 (2004) 139–174. doi:10.1021/cr020357g.

[5] J.C. Goldschmidt, S. Fischer, Upconversion for Photovoltaics - a Review of Materials, Devices and Concepts for Performance Enhancement, Adv. Opt. Mater. 3 (2015) 510–535. doi:10.1002/adom.201500024.

[6] J. Zhou, Q. Liu, W. Feng, Y. Sun, F. Li, Upconversion Luminescent Materials: Advances and Applications, Chem. Rev. 115 (2015) 395–465. doi:10.1021/cr400478f.

[7] A. Sarakovskis, J. Grube, A. Mishnev, M. Springis, Up-conversion processes in $NaLaF_4:Er^{3+}$, Opt. Mater. (Amst). 31 (2009) 1517–1524. doi:10.1016/j.optmat.2009.02.015.

[8] J.L. Sommerdijk, Influence of host lattice on the infrared-excited visible luminescence in Yb^{3+}, Er^{3+}-doped fluorides, J. Lumin. 6 (1973) 61–67. doi:10.1016/0022-2313(73)90095-1.

[9] C. Renero-Lecuna, R. Martín-Rodríguez, R. Valiente, J. González, F. Rodríguez, K.W. Krämer, H.U. Güdel, Origin of the High Upconversion Green Luminescence Efficiency in β-$NaYF_4$: 2%Er^{3+}, 20%Yb^{3+}, Chem. Mater. 23 (2011) 3442–3448. doi:10.1021/cm2004227.

[10] F. Shi, J. Wang, X. Zhai, D. Zhao, W. Qin, Facile synthesis of β-$NaLuF_4$: Yb/Tm hexagonal nanoplates with intense ultraviolet upconversion luminescence, CrystEngComm. 13 (2011) 3782. doi:10.1039/c1ce05092c.

[11] a. de Pablos-Martín, G.C. Mather, F. Muñoz, S. Bhattacharyya, T. Höche, J.R. Jinschek, T. Heil, A. Durán, M.J. Pascual, Design of oxy-fluoride glass-ceramics containing $NaLaF_4$ nano-crystals, J. Non. Cryst. Solids. 356 (2010) 3071–3079. doi:10.1016/j.jnoncrysol.2010.04.057.

[12] E. Elsts, G. Krieke, U. Rogulis, K. Smits, A. Zolotarjovs, J. Jansons, A. Sarakovskis, K. Kundzins, Rare earth doped glass–ceramics containing $NaLaF_4$ nanocrystals, Opt. Mater. (Amst). 59 (2016) 130–135. doi:10.1016/j.optmat.2016.01.005.

[13] A. Herrmann, M. Tylkowski, C. Bocker, C. Rüssel, Cubic and Hexagonal $NaGdF_4$ Crystals Precipitated from an Aluminosilicate Glass: Preparation and Luminescence Properties, Chem. Mater. 25 (2013) 2878–2884. doi:10.1021/cm401454y.

[14] D. Chen, Z. Wan, Y. Zhou, P. Huang, J. Zhong, M. Ding, W. Xiang, X. Liang, Z. Ji, Bulk glass ceramics containing Yb^{3+}/Er^{3+}: β-$NaGdF_4$ nanocrystals: Phase-separation-controlled crystallization, optical spectroscopy and upconverted temperature sensing

behavior, J. Alloys Compd. 638 (2015) 21–28. doi:10.1016/j.jallcom.2015.02.170.

[15] A. Sarakovskis, G. Krieke, Upconversion luminescence in erbium doped transparent oxyfluoride glass ceramics containing hexagonal $NaYF_4$ nanocrystals, J. Eur. Ceram. Soc. 35 (2015) 3665–3671. doi:10.1016/j.jeurceramsoc.2015.06.014.

[16] Y. Gao, Y. Hu, P. Ren, D. Zhou, J. Qiu, Phase transformation and enhancement of luminescence in the Tb^{3+}-Yb^{3+} co-doped oxyfluoride glass ceramics containing $NaYF_4$ nanocrystals, J. Eur. Ceram. Soc. 36 (2016) 2825–2830. doi:10.1016/j.jeurceramsoc.2016.04.027.

[17] F. Liu, E. Ma, D. Chen, Y. Yu, Y. Wang, Tunable Red-Green Upconversion Luminescence in Novel Transparent Glass Ceramics Containing Er:$NaYF_4$ Nanocrystals, J. Phys. Chem. B. 110 (2006) 20843–20846. doi:10.1021/jp063145m.

[18] F. Liu, Y. Wang, D. Chen, Y. Yu, Investigation on crystallization kinetics and microstructure of novel transparent glass ceramics containing Nd:$NaYF_4$ nano-crystals, Mater. Sci. Eng. B. 136 (2007) 106–110. doi:10.1016/j.mseb.2006.09.012.

[19] F. Liu, D. Chen, Y. Wang, E. Ma, Y. Yu, Spectroscopic calculation of $NaYF_4$ contained transparent glass ceramics doped with different content of Nd^{3+}, J. Alloys Compd. 443 (2007) 143–148. doi:10.1016/j.jallcom.2006.09.124.

[20] X. Li, H. Guo, Y. Wei, Y. Guo, H. Lu, H.M. Noh, J.H. Jeong, Enhanced up-conversion in Er^{3+}-doped transparent glass-ceramics containing $NaYbF_4$ nanocrystals, J. Lumin. 152 (2014) 168–171. doi:10.1016/j.jlumin.2013.11.042.

[21] Y. Wei, X. Liu, X. Chi, R. Wei, H. Guo, Intense upconversion in novel transparent $NaLuF_4$:Tb^{3+}, Yb^{3+} glass–ceramics, J. Alloys Compd. 578 (2013) 385–388. doi:10.1016/j.jallcom.2013.06.014.

[22] D. Chen, Y. Zhou, Z. Wan, P. Huang, H. Yu, H. Lu, Z. Ji, Enhanced upconversion luminescence in phase-separation-controlled crystallization glass ceramics containing Yb/Er(Tm): $NaLuF_4$ nanocrystals, J. Eur. Ceram. Soc. 35 (2015) 2129–2137. doi:10.1016/j.jeurceramsoc.2015.01.021.

[23] R.E. Thoma, H. Insley, G.M. Hebert, The Sodium Fluoride-Lanthanide Trifluoride

Systems, Inorg. Chem. 5 (1966) 1222–1229. doi:10.1021/ic50041a032.

[24] O. Janka, T. Schleid, Facile Synthesis of Bastnaesite -Type LaF[CO_3] and Its Thermal Decomposition to LaOF for Bulk and Eu^{3+} -Doped Samples, Eur. J. Inorg. Chem. 2009 (2009) 357–362. doi:10.1002/ejic.200800931.

[25] D. Louër, A. Boultif, Powder pattern indexing and the dichotomy algorithm, in: Zeitschrift Fur Krist. Suppl., 2007: pp. 191–196. doi:10.1524/zksu.2007.2007.suppl_26.191.

[26] J. Rodríguez-carvajal, Recent developments for the program FULLPROF, Newsletter in Commission on Powder Diffraction (IUCr). 26, (2001) 12-19.

[27] A. de Pablos-Martín, A. Durán, M.J. Pascual, Nanocrystallisation in oxyfluoride systems: mechanisms of crystallisation and photonic properties, Int. Mater. Rev. 57 (2012) 165–186. doi:10.1179/1743280411Y.0000000004.

[28] W. Vogel, Phase separation in glass, J. Non. Cryst. Solids. 24 (1977) 170–214. doi:10.1016_0022-3093(77)90093-x.

[29] C. Bocker, J. Wiemert, C. Rüssel, The formation of strontium fluoride nano crystals from a phase separated silicate glass, J. Eur. Ceram. Soc. 33 (2013) 1737–1745. doi:10.1016/j.jeurceramsoc.2013.02.008.

[30] J. Zhao, R. Ma, X. Chen, B. Kang, X. Qiao, J. Du, X. Fan, U. Ross, C. Roiland, A. Lotnyk, L. Kienle, X. Zhang, From Phase Separation to Nanocrystallization in Fluorosilicate Glasses: Structural Design of Highly Luminescent Glass-Ceramics, J. Phys. Chem. C. 120 (2016) 17726–17732. doi:10.1021/acs.jpcc.6b05796.

[31] I. V. Veksler, A.M. Dorfman, P. Dulski, V.S. Kamenetsky, L. V. Danyushevsky, T. Jeffries, D.B. Dingwell, Partitioning of elements between silicate melt and immiscible fluoride, chloride, carbonate, phosphate and sulfate melts, with implications to the origin of natrocarbonatite, Geochim. Cosmochim. Acta. 79 (2012) 20–40. doi:10.1016/j.gca.2011.11.035.

[32] J.P.M. van der Meer, R.J.M. Konings, D. Sedmidubský, A.C.G. van Genderen, H. a. J. Oonk, Calorimetric analysis of NaF and $NaLaF_4$, J. Chem. Thermodyn. 38 (2006)

1260–1268. doi:10.1016/j.jct.2006.03.002.

[33] S. Chen, S. Zhao, F. Zheng, C. Zhang, L. Huang, S. Xu, Enhanced up-conversion luminescence of Er^{3+}:LaOF oxyfluoride borosilicate glass ceramics, Ceram. Int. 39 (2013) 2909–2913. doi:10.1016/j.ceramint.2012.09.065.

[34] S.L. Kang, X.Q. Song, X.J. Huang, J.R. Qiu, G.P. Dong, Enhanced emission and spectroscopic properties in oxyfluoride glass ceramics containing LaOF:Er^3+ nanocrystals, Opt. Mater. Express. 6 (2016) 2351. doi:10.1364/OME.6.002351.

[35] I. V. Veksler, A.M. Dorfman, M. Kamenetsky, P. Dulski, D.B. Dingwell, Partitioning of lanthanides and Y between immiscible silicate and fluoride melts, fluorite and cryolite and the origin of the lanthanide tetrad effect in igneous rocks, Geochim. Cosmochim. Acta. 69 (2005) 2847–2860. doi:10.1016/j.gca.2004.08.007.

[36] B.P. Sobolev, Non-stoichiometry in inorganic fluorides and phases with fluorite structure, Butll. Soc. Cat. Cien. J. 12 (1991) 275–332.

[37] R.D. Shannon, Revised effective ionic radii and systematic studies of interatomic distances in halides and chalcogenides, Acta Crystallogr. Sect. A. 32 (1976) 751–767. doi:10.1107/S0567739476001551.

[38] M. Pollnau, D.R. Gamelin, S.R. Lüthi, H.U. Güdel, M.P. Hehlen, Power dependence of upconversion luminescence in lanthanide and transition-metal-ion systems, Phys. Rev. B. 61 (2000) 3337–3346. doi:10.1103/PhysRevB.61.3337.

[39] A. Aebischer, M. Hostettler, J. Hauser, K. Krämer, T. Weber, H.U. Güdel, H.-B. Bürgi, Structural and Spectroscopic Characterization of Active Sites in a Family of Light-Emitting Sodium Lanthanide Tetrafluorides, Angew. Chemie Int. Ed. 45 (2006) 2802–2806. doi:10.1002/anie.200503966.

[40] A. Sarakovskis, G. Krieke, G. Doke, J. Grube, L. Grinberga, M. Springis, Comprehensive study on different crystal field environments in highly efficient $NaLaF_4$:Er^{3+} upconversion phosphor, Opt. Mater. (Amst). 39 (2015) 90–96. doi:10.1016/j.optmat.2014.11.004.

Figure captions

Fig. 1. DTA curves of glasses doped with 1% ErF_3 and 0, 1 and 3% YbF_3.

Fig. 2. XRD patterns of glass ceramics heat treated at 600^0C for 1 h.

Fig. 3. XRD patterns of glasses and glass ceramics heat treated at different temperatures for 1 h doped with a) 0% YbF_3 and b) 3% YbF_3.

Fig. 4. SEM micrographs of glass and glass ceramics heat treated at 600-800^{o}C for 1 h doped with (a-d) 0% YbF_3 and (e-f) 3% YbF_3.

Fig. 5. TEM micrographs and selected area diffraction patterns of a-c) glass and d-f) glass ceramics doped with 3% YbF_3 heat treated at 600^0C for 1 h.

Fig. 6. Photographs of the glass and glass ceramics doped with 2% YbF_3 a) as prepared and b) excited at 975 nm.

Fig. 7. a) UCL spectra of Er^{3+} ions in the glass ceramics with 1% ErF_3 and 0-3% YbF_3 heat treated at 600^0C for 1 h excited at 978 nm. Inset: The dependence of UCL green emission decay time on the YbF_3 content in glass ceramics. b) Partial energy level scheme of Er^{3+} and Yb^{3+} and the possible UCL mechanisms.

Fig. 8. Power dependence of UCL intensity of a) $^4S_{3/2}\rightarrow{}^4I_{15/2}$ (green), $^4F_{9/2}\rightarrow{}^4I_{15/2}$ (red) and b) $^2H_{9/2}\rightarrow{}^4I_{15/2}$ (violet), $^4G_{11/2}\rightarrow{}^4I_{15/2}$ (ultraviolet) emission in the glass ceramics with 2% YbF_3.

Fig. 9. UCL spectra of Er^{3+} green emission excited at 978 nm of glass and glass ceramics heat treated at 500-800^{0}C for 1 h doped with 1% ErF_3 and a) 0% YbF_3 and b) 3% YbF_3. Lower section: upconversion luminescence spectra of erbium doped polycrystalline $NaLaF_4$ and LaF_3 excited at 978 nm.

Fig. 10. a) excitation spectra (exciting $^4F_{7/2}$, detecting green emission) and b) the green emission spectra (excited at 486 nm) of Er^{3+} ions in the glass ceramics with 1% ErF_3 and 0% YbF_3 heat treated at 600^0C for 1 h compared with the polycrystalline $NaLaF_4$ measured at 10 K.

Fig. 11. Luminescence spectra of Er^{3+} ions in glass ceramics with 1% ErF_3 and 0% YbF_3 heat treated at 600^0C for 1 h detected at 10 K.

Fig. 12. a) Luminescence excitation spectra of Er^{3+} (exciting $^4F_{7/2}$, detecting green emission) in LaOF compared with the glass ceramics doped with 1% ErF_3 and 3% YbF_3 heat treated at 500°C for 1 h, monitoring green emission at 10 K and b) Luminescence spectra of Er^{3+} green emission in LaOF compared with the glass ceramics excited at the maximal intensity of each compound monitored at 10 K.

Fig. 13. Lattice parameter of α-$NaREF_4$ phases with variable NaF-REF_3 ratio according to [23]. Ionic radii taken from [37]. Inset: lattice parameter of fluorite phase in glass ceramics heat treated at 500-600^{0}C for 1h.

Fig. 14. a) Luminescence excitation spectra of Er^{3+} in α-$NaYF_4$ compared with the glass ceramics (3% YbF_3) heat treated at 500°C for 1 h, monitoring green emission at 10 K and b) luminescence spectra of Er^{3+} green emission in α-$NaYF_4$ compared with the glass ceramics monitored at 10 K.

Table 1

Thermal properties of oxyfluoride glasses

YbF_3 (mol%)	T_g (°C)	T_{c1} (°C)	T_{tr} (°C)
0%	460±1	630±1	-
1%	480±1	600±1	765±1
3%	500±1	420±1	760±1

Table 2

The crystalline phases in glass and glass ceramics with 0% and 3% YbF_3

Heat treatment	YbF_3 content in the precursor glass (mol%)	
	0%	3%
-	amorphous	amorphous
500°C for 1 h	amorphous	$NaLaF_4$+fluorite
600°C for 1 h	$NaLaF_4$	$NaLaF_4$+fluorite
700°C for 1 h	$NaLaF_4$+$NaAlSiO_4$	$NaLaF_4$+fluorite+LaF_3
800°C for 1 h	$NaAlSiO_4$	fluorite+ LaF_3

Figure 1

Click here to download high resolution image

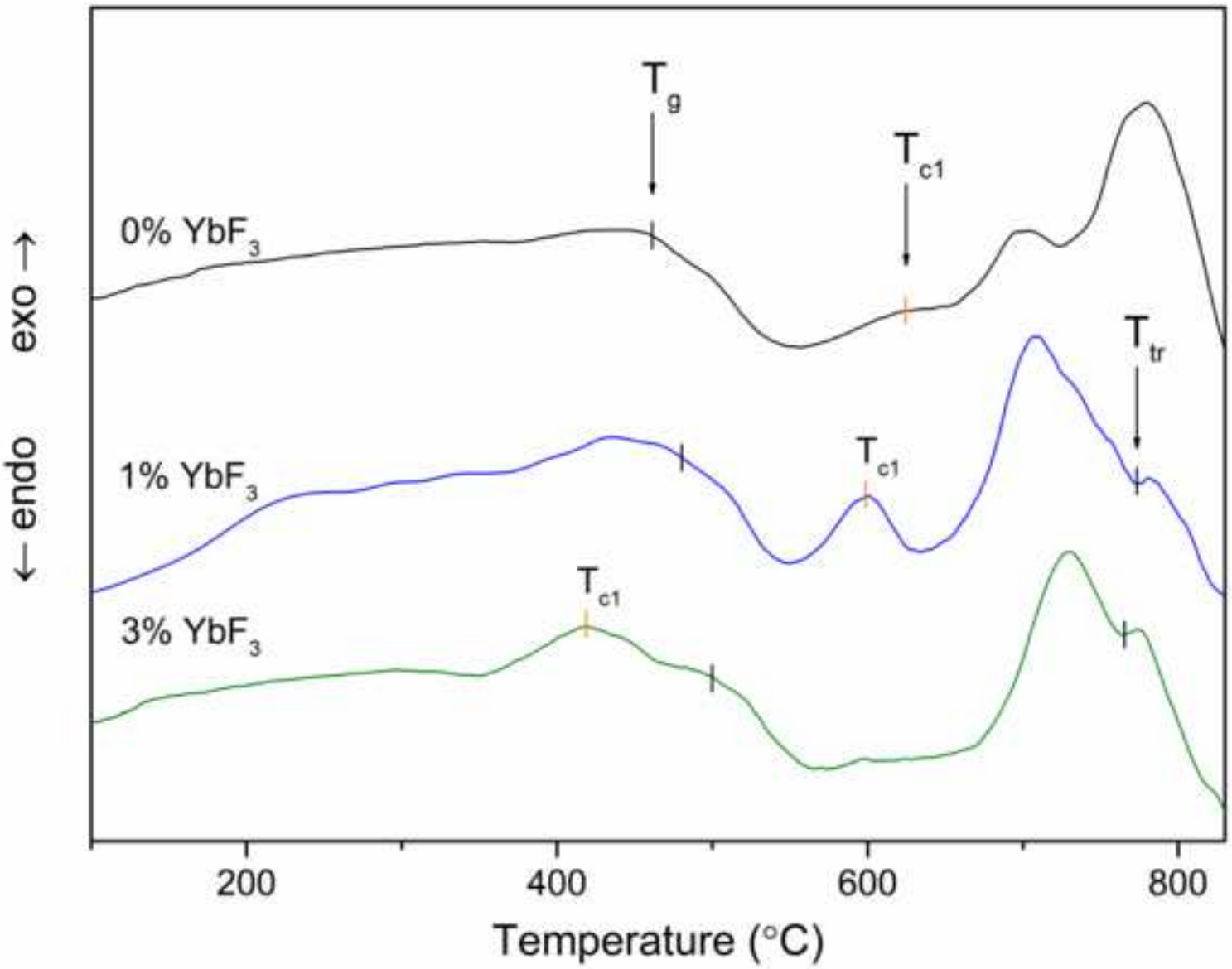

Figure 2

Click here to download high resolution image

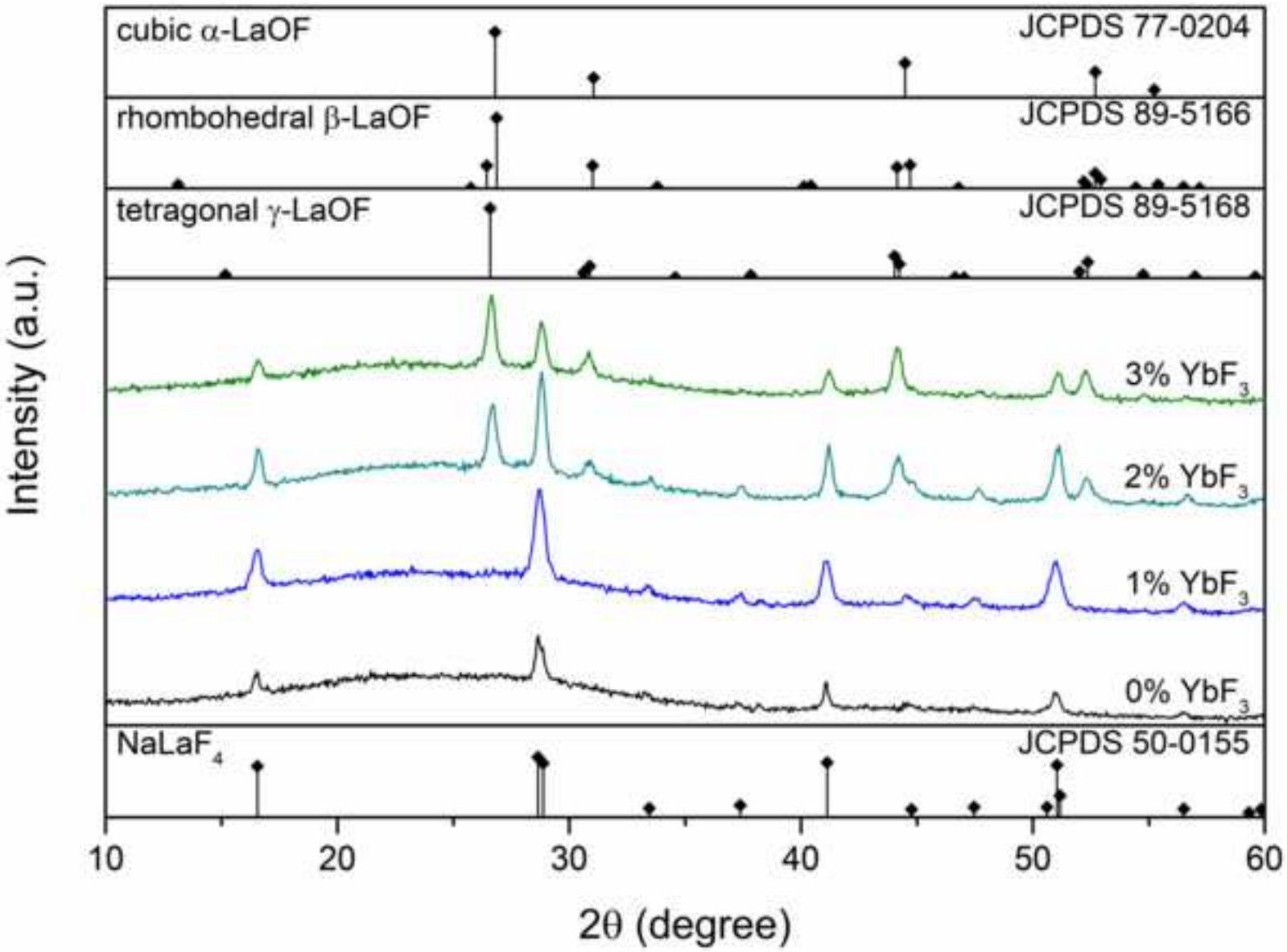

Figure 3

Click here to download high resolution image

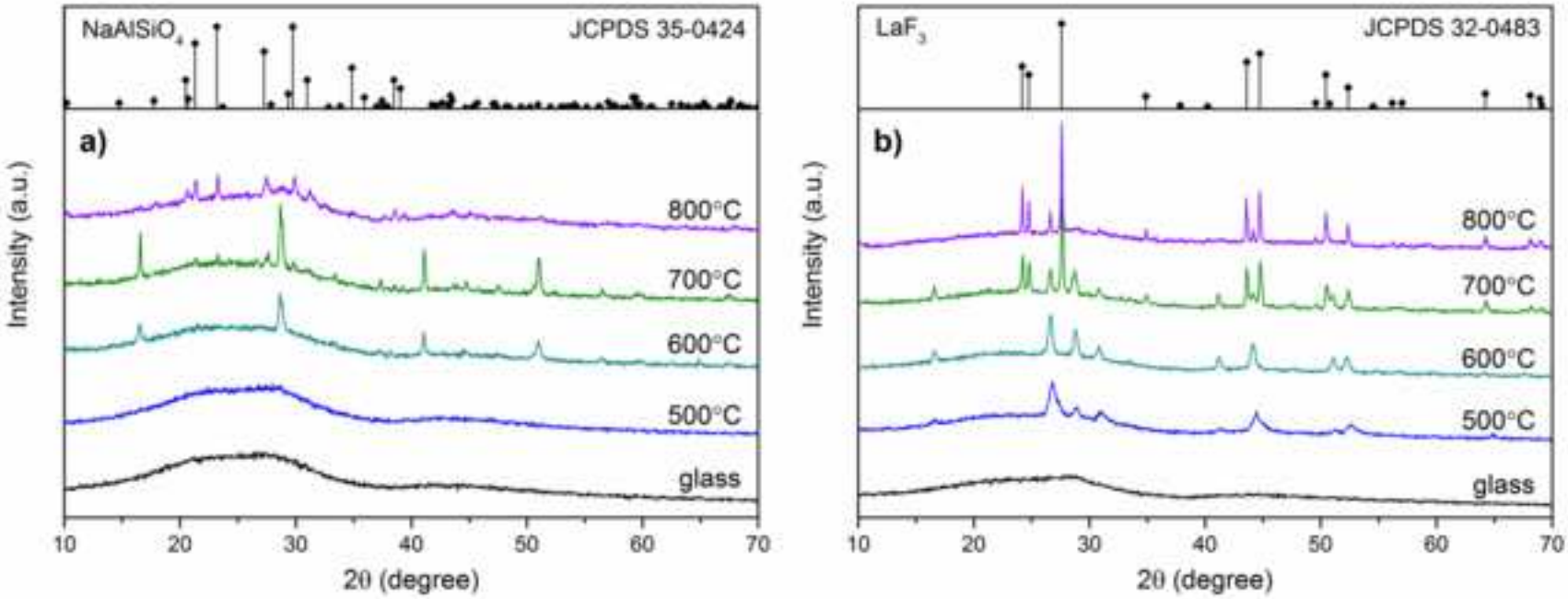

Figure 4

Click here to download high resolution image

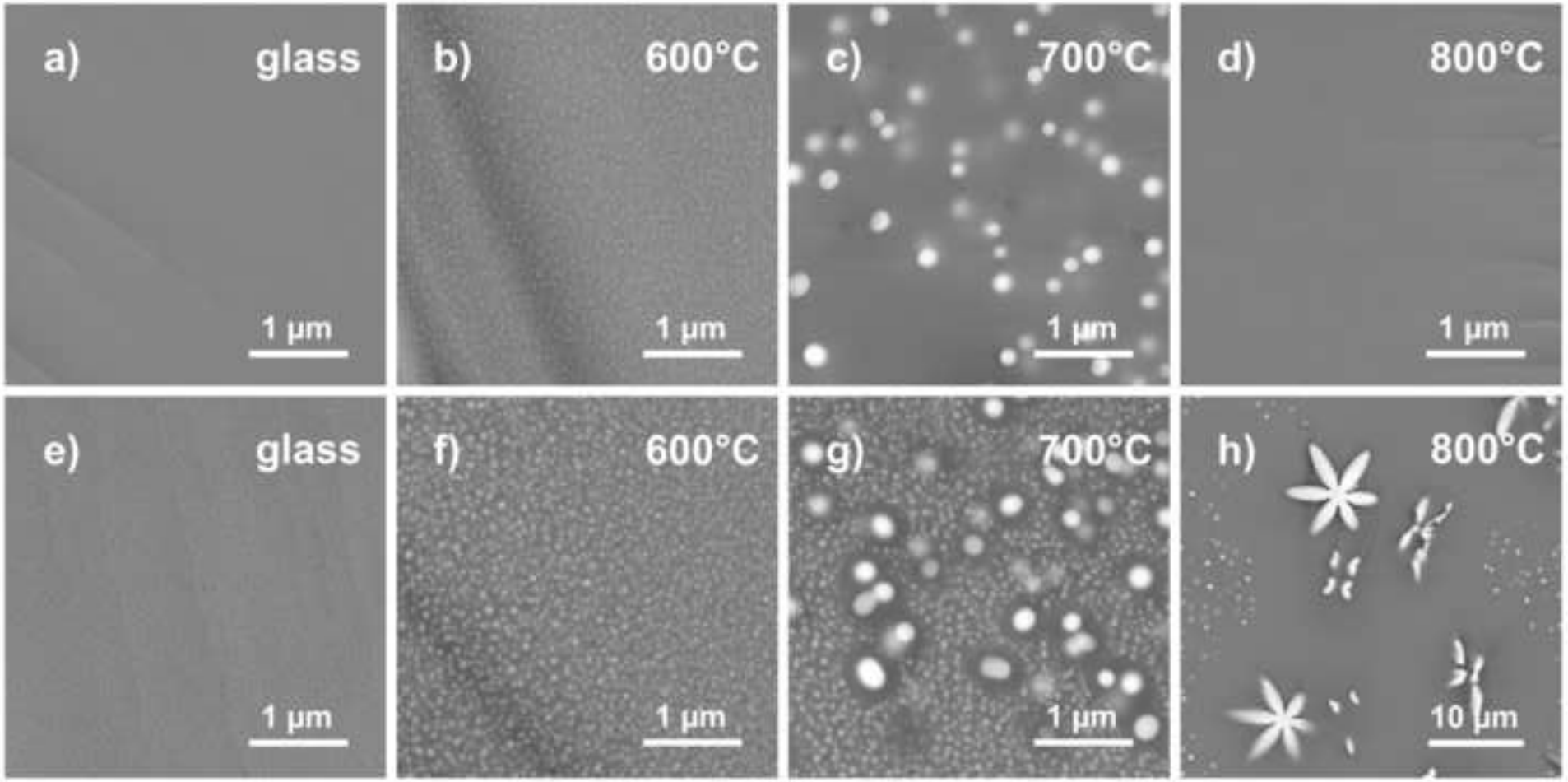

Figure 5
Click here to download high resolution image

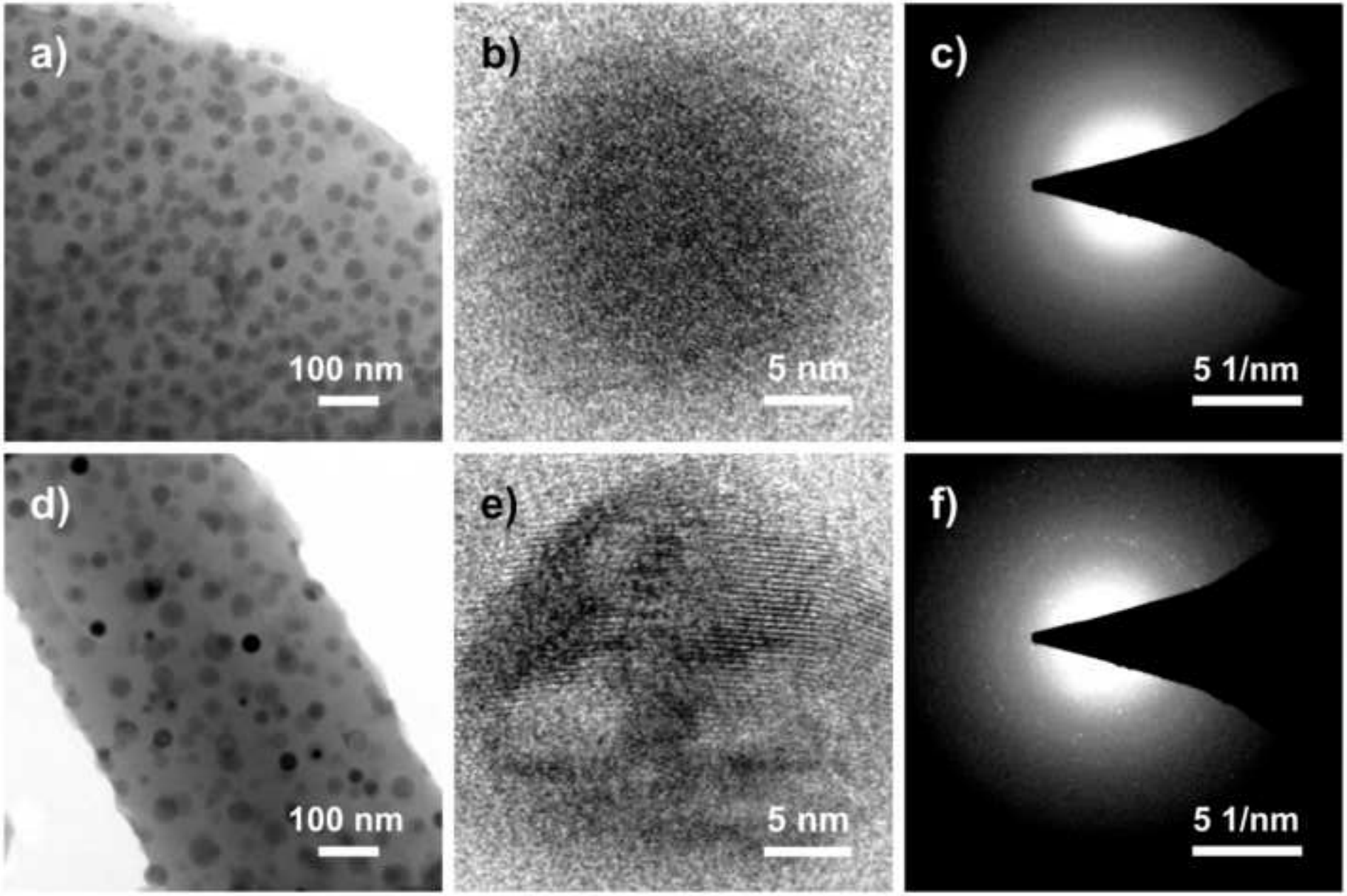

Figure 6
Click here to download high resolution image

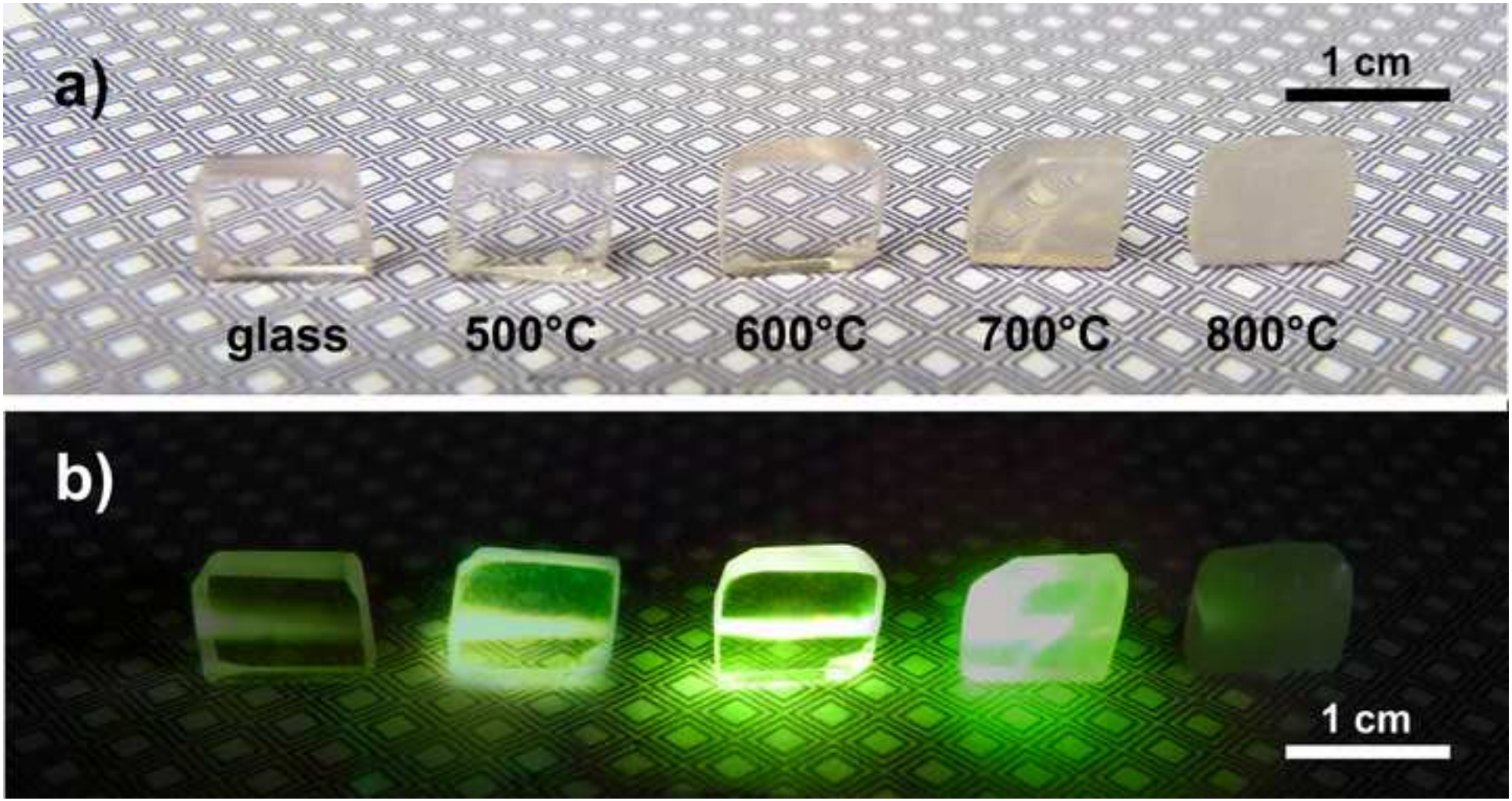

Figure 7

Click here to download high resolution image

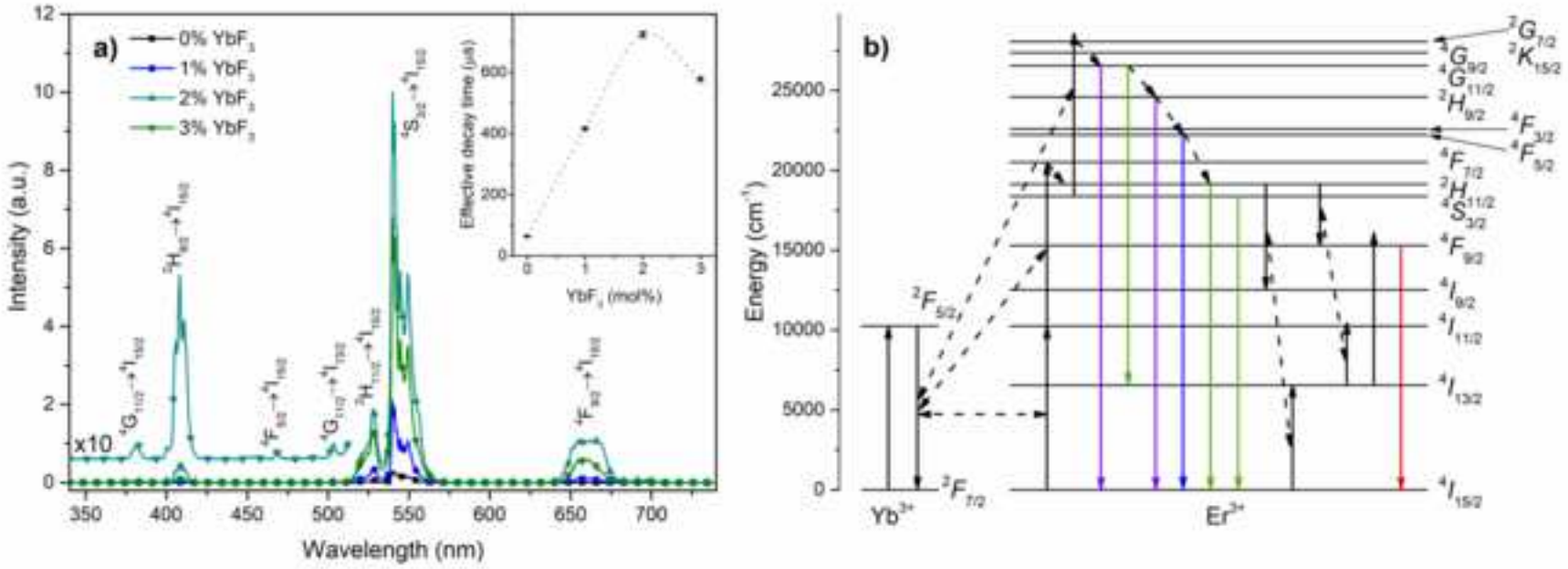

Figure 8

Click here to download high resolution image

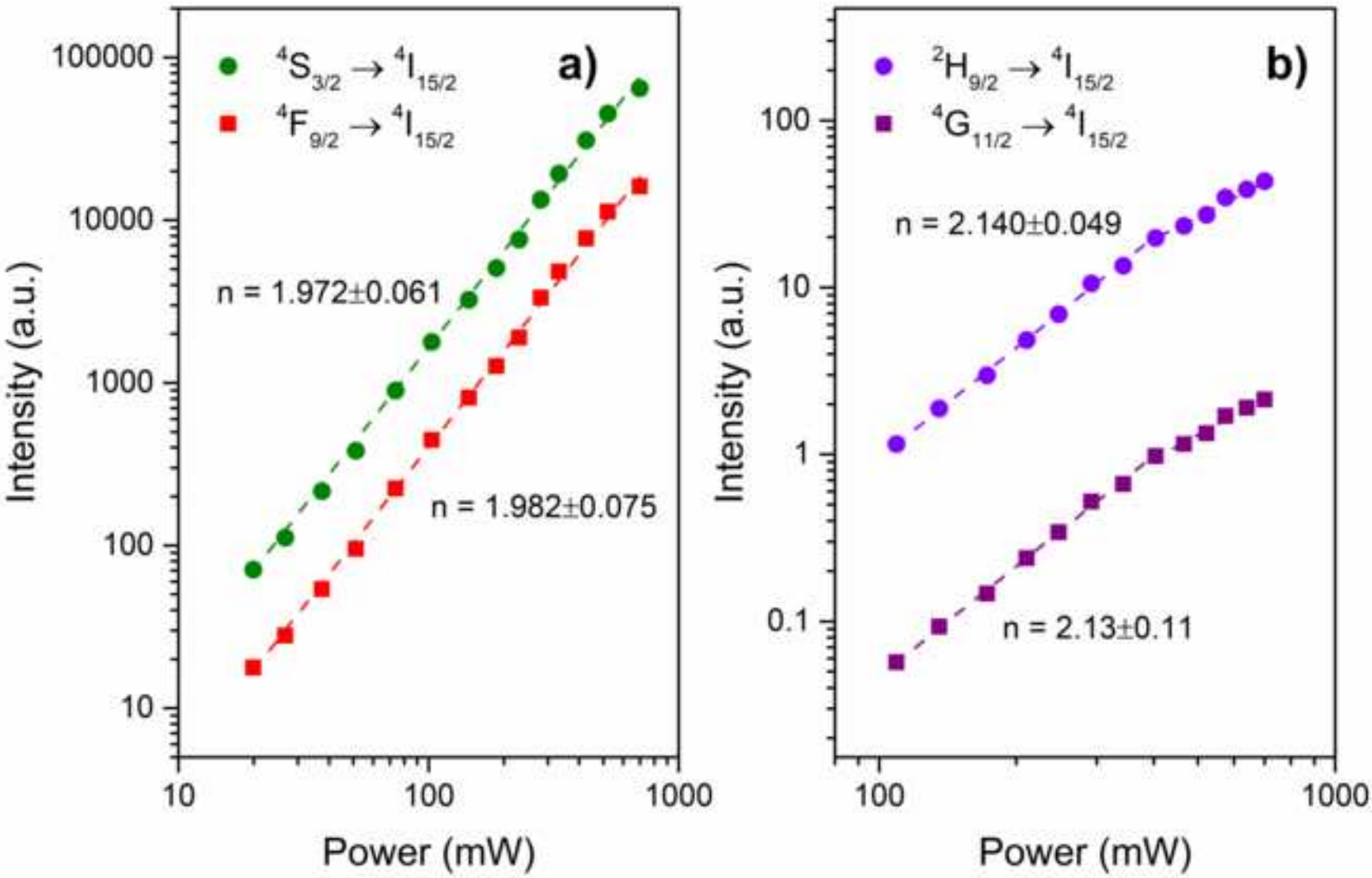

Figure 9

Click here to download high resolution image

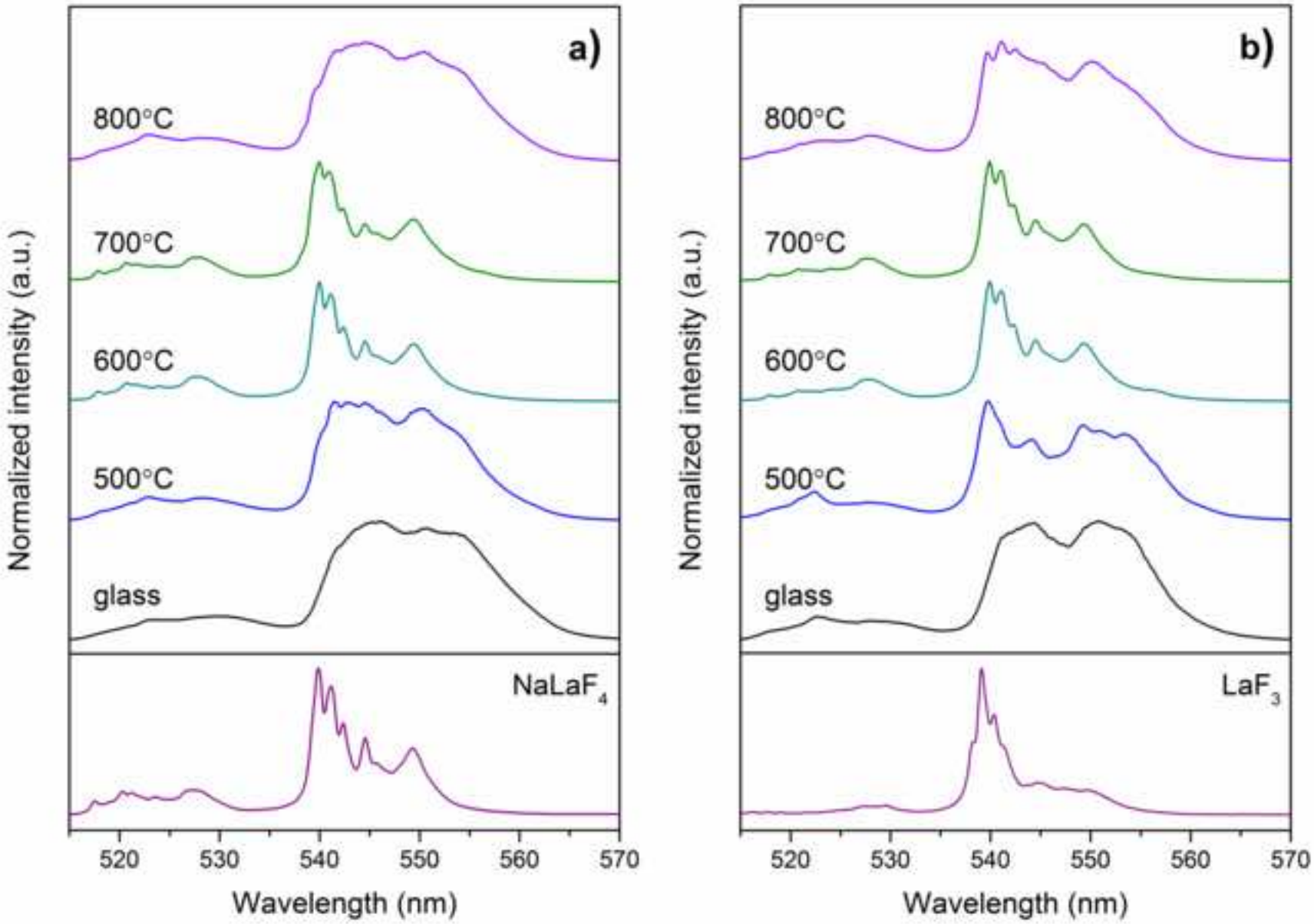

Figure 10
Click here to download high resolution image

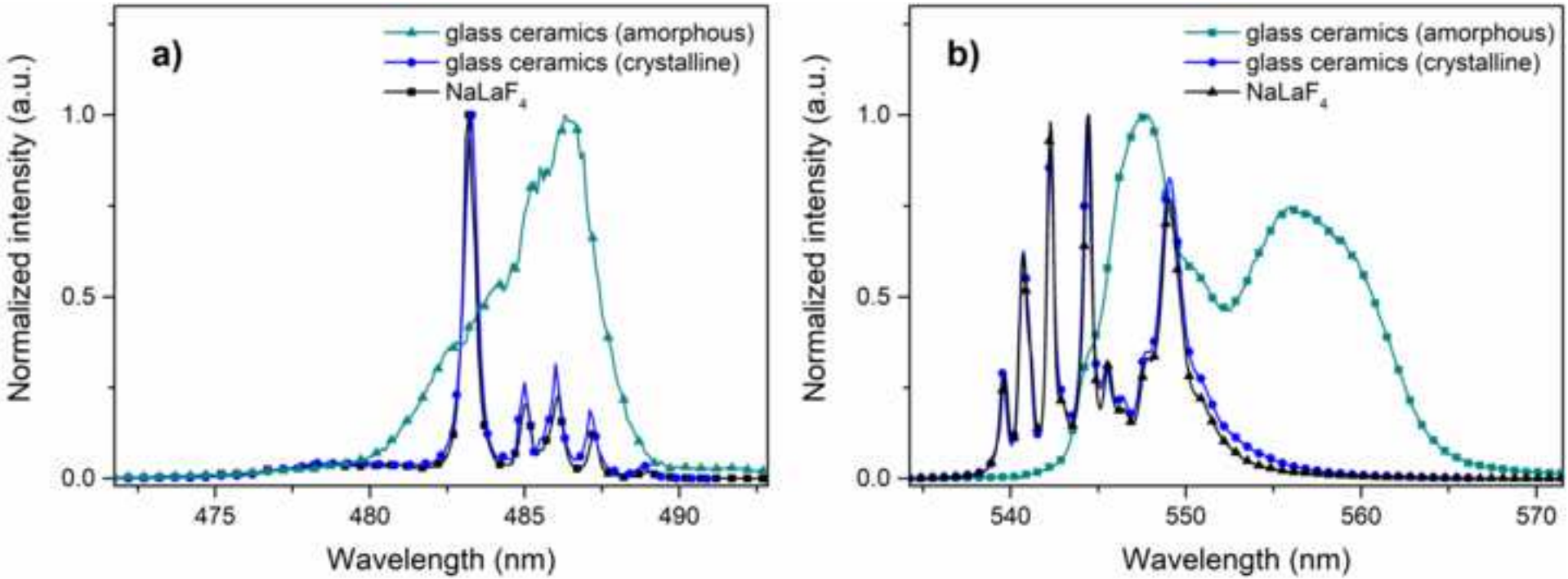

Figure 11

Click here to download high resolution image

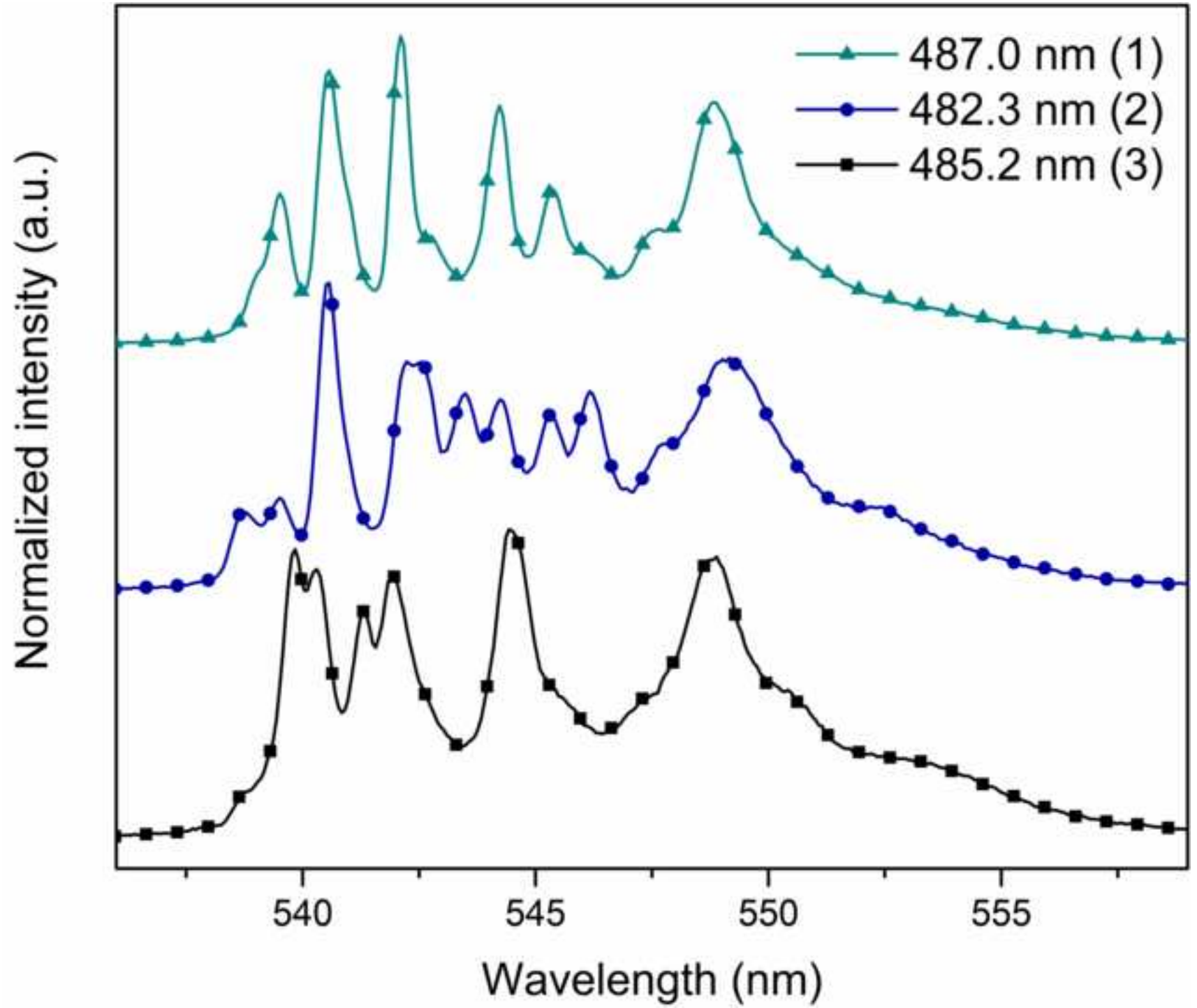

Figure 12

Click here to download high resolution image

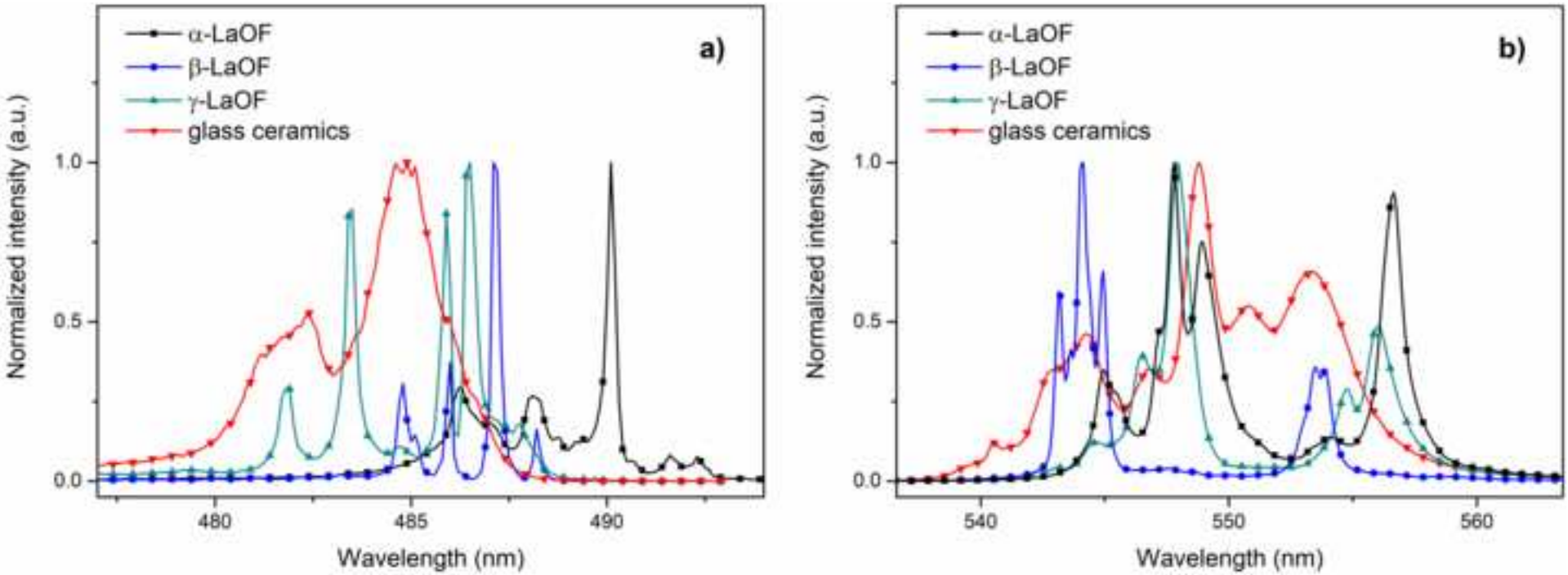

Figure 13

Click here to download high resolution image

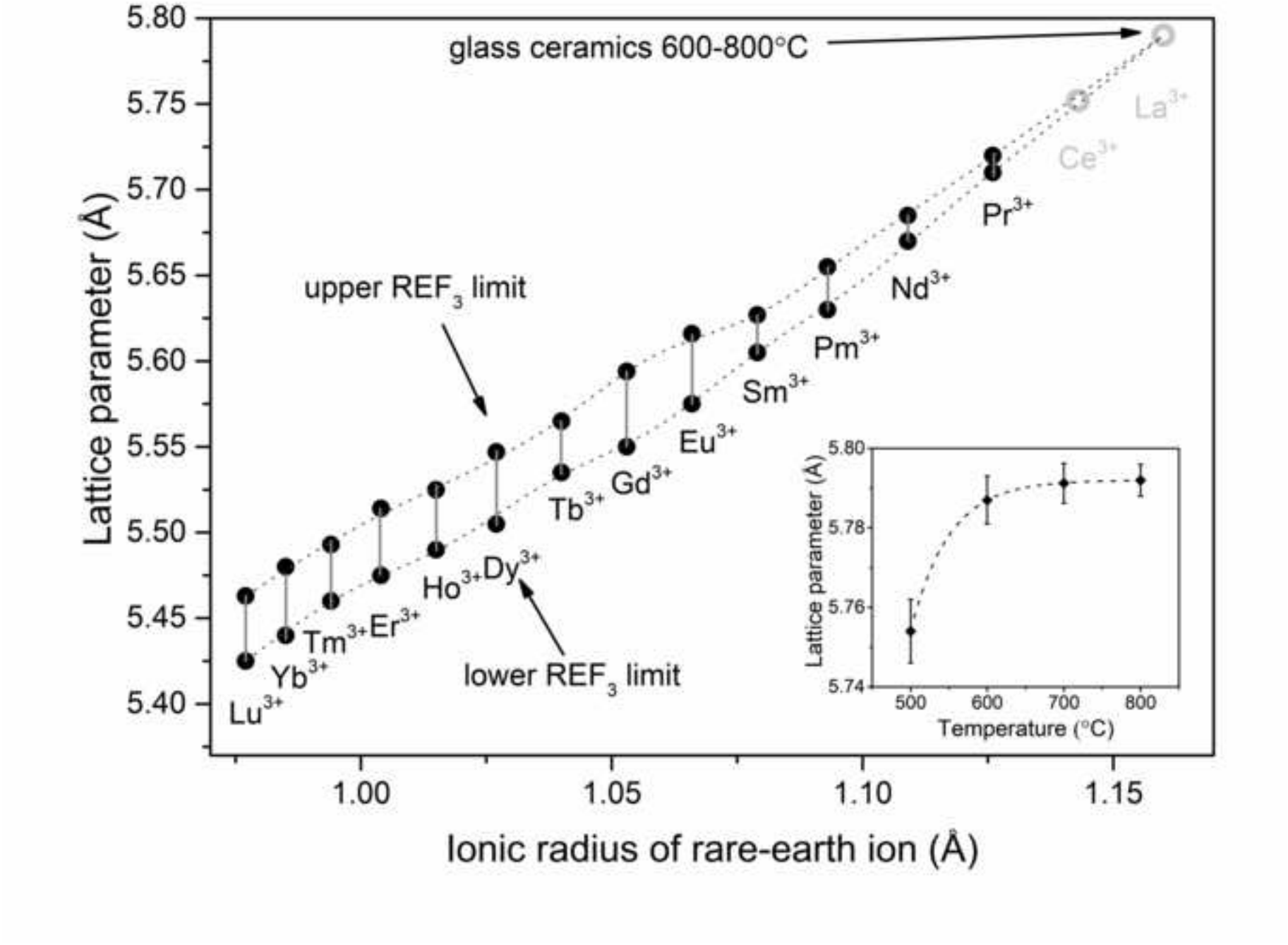

Figure 14
Click here to download high resolution image

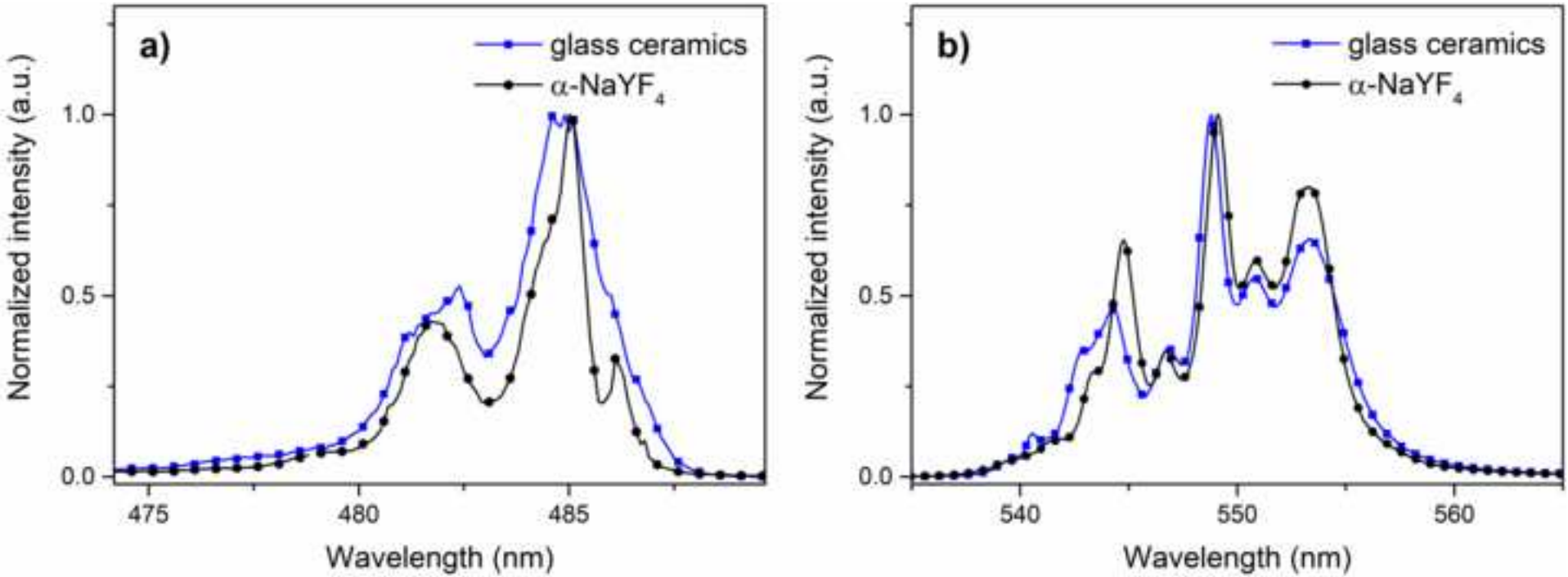

Institute of Solid State Physics, University of Latvia as the Center of Excellence has received funding from the European Union's Horizon 2020 Framework Programme H2020-WIDESPREAD-01-2016-2017-TeamingPhase2 under grant agreement No. 739508, project CAMART²